DOI: 10.1002/ ((please add manuscript number))
Article type: Progress Report

Influence of Radiation on the Properties and the Stability of Hybrid Perovskites

Felix Lang, Oleksandra Shargaieva, Viktor V. Brus, Heinz C. Neitzert, Jörg Rappich, and Norbert H. Nickel*

F. Lang, O. Shargaieva, Dr. V. V. Brus, Dr. J. Rappich, Prof. Dr. N. H. Nickel,
Helmholtz-Zentrum Berlin für Materialien und Energie GmbH, Institut für Silizium Photovoltaik, Kekuléstr. 5, 12489 Berlin, Germany.
E-mail: felix.lang@helmholtz-berlin.de

Prof. Dr. H. C. Neitzert
Department of Industrial Engineering (DIIn), Salerno University, Via Giovanni Paolo II 132, 84084 Fisciano, SA, Italy.

Keywords: perovskite, solar cells, radiation, stability, defects

Organic-inorganic perovskites are ideal for optoelectronic applications. In particular, perovskite single and perovskite tandem solar cells with silicon are close to their market entry. Despite their swift rise in efficiency to more than 21 %, solar cell lifetimes are way below the needed 25 years. In fact, comparison of the T_{80} lifetime of numerous solar cells throughout literature reveals a strongly reduced stability under illumination. The various detrimental effects are discussed. Most notably, moisture and heat related degradation can be mitigated easily by now. Recently however, several photo-induced degradation mechanisms have been observed. Under illumination alloyed perovskites tend to phase segregate, while further, oxygen catalyzes deprotonation of the organic cations. Additionally, during illumination photo-generated charge can be trapped in the N-H antibonding orbitals causing the dissociation of the organic cation. On the other hand, organic-inorganic perovskites exhibit a high radiation hardness that is superior to crystalline silicon. This progress report thoroughly reviews proposed degradation mechanisms reported in literature and discusses the microscopic mechanisms and their implications for solar cells.

1. Introduction

Exceptional electronic and optical properties attracted great interest in organic-inorganic perovskites within the last years. Because of their direct band-gap, large absorption coefficient [1], low defect concentration [2] and large diffusion lengths [3,4] this material class is ideal for optoelectronics. Applications range from efficient light emitting diodes [5–13] and lasers [14–23] to photodetectors [24–40] and solar cells. Today's best performing solar cells exceed power conversion efficiencies (η) of 21%. [41,42] In fact, organic-inorganic perovskites outperform silicon solar cells already in terms of their potential loss (difference between V_{OC} and band-gap), as they are not limited by Auger recombination.[41] The tunable band-gap energy makes the material class further highly attractive for tandem solar cells. [43] The combination of the high band-gap perovskite and a low band-gap semiconductor such as silicon allows to compensate for thermalization losses. Efficiencies are close to outperform the respective single junctions [44–46] and realistic estimates with over 28 % power conversion efficiency (η) are within reach. [47] However, organic-inorganic perovskites tend to degrade under numerous conditions. [48–53] To be more specific, degradation of organic-inorganic perovskites has been observed under illumination [54–59], at elevated temperatures [60–66], under bias [67–69], in moisture [64,70–87], in oxygen [54,58,77,88,89], and under high-energy irradiation [90–93]. The reported solar cell lifetimes are typically less than 2000 hrs. [94] Commercially available silicon solar cells, on the other hand, maintain over 85 % of their initial efficiency over a course of 25 years. For a true commercial success, this time span has to be reached for any new material class. In particular, stability is essential for high power perovskite single junctions and tandem solar cells combining perovskites with silicon.

In this review we revisit the degradation of organic-inorganic perovskites. First, we present an overview of the current state of device stability. Considering over 50 publications, we are able to observe two trends: (i) An increase in the reported device stability within the last years and (ii) a severe mismatch of reported lifetimes between storage in the dark or under illumination. Then, we focus on the degradation mechanisms of organic-inorganic perovskites prepared from methylammonium and formamidinium lead iodide, which are the two compounds most commonly used. We will show that moisture and heat are two important degradation channels that are both well understood and resolved. Then, the focus will shift on two recently identified degradation channels that are observed during irradiation with light and high-energy particles. The exact details of the degradation mechanisms are still being discussed

controversially. Based on recent publications and tailored experiments we will show that photo-induced defect formation is the Achilles heel of organic-inorganic perovskite solar cells. As there are no brilliant solutions yet, we will propose routes to go beyond organic-inorganic perovskites.

2. Instability of Perovskite Solar cells

The very first perovskite solar cells were based on methylammonium (MA) lead iodide (**(**$MAPbI_3$) quantum dots within a nanocrystalline TiO_2 matrix. The used liquid electrolyte induced a swift dissolution of the perovskite. [95] Substitution with a solid-state hole conductor enabled a first improvement in stability from minutes to hours. [96] With the vast increase of research effort, perovskite solar-cell efficiencies along with their stability increased vastly. **Figure 1** depicts the evolution of reported solar-cell lifetimes as a function of their efficiency and their publication year.[41–43,46,64,73,81,84,95–141] More precisely, the graph depicts the T_{80} lifetime to allow accurate comparison. This lifetime is defined as the time until the efficiency of the device decreases to 80 % of its initial value. [142] Blue and orange columns correspond to devices stored under dark and light conditions (100 $mWcm^{-2}$), respectively. Figure 1 reflects the leaping trend of the efficiency vs. year. [143] Considering devices stored under dark conditions only, a vast increase of the T_{80} lifetime over time is obvious (blue columns). Record T_{80} lifetimes reach 4500 hours. [104] This achievement is a result of improved device encapsulation and/or superior barrier layers. The improved devices often include hydrophobic hole transport layers [73,84,97,99,103,107,109,112,120,121,126,144,145], inorganic barrier layers [104,131,135], PEDOT:PSS additives ensuring a neutral pH value [110,124], inorganic charge selective contacts [108,117,121,123,129,135,137,138] and perovskite additives [73,111] to name a few. Apart from that, compositional changes of the perovskite itself are important. Indeed, various organic and inorganic cations, as well as combinations thereof, have been explored recently. [41,81,146,147]

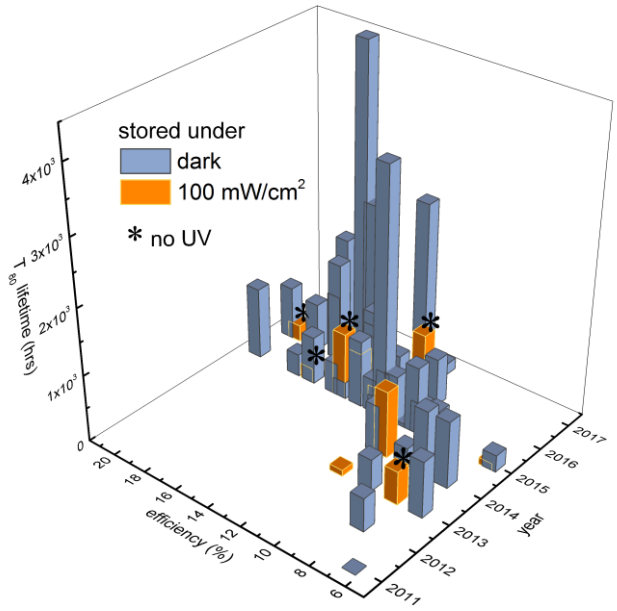

Figure 1. Evolution of the T_{80} lifetime of perovskite solar cells as a function of their initial efficiency and the publication year. Blue and orange columns refer to devices stored in the

dark or under illumination with a light intensity of 100 mWcm^{-2}, respectively. Asterisks refer to studies performed under reduced UV illumination. [41–43,46,64,73,81,84,95–141]

Intriguingly, T_{80} lifetimes are considerably shorter for devices exposed to continuous illumination with a power density of 100 mWcm^{-2} (orange columns in figure 1). Under these conditions record lifetimes reach 1000 hours only.[46] This is far below the set target of 25 years of outdoor operation with over 30,000 sun hours. [Note that this calculation is based on the yearly sum of the global irradiation in Berlin (52° north).] It has to be mentioned that various record lifetimes were collected under illumination with reduced or no UV irradiation. The corresponding data are marked with an asterisk in figure 1. However, the blue to ultraviolet part of the solar spectrum is not negligible and triggers the dissociation of organic cations.[139,144,148] Moreover, oxygen vacancies are activated within the widely used TiO_2 layers under UV illumination. [139,144] The underlying mechanisms are discussed in chapter 3.3. Therefore, for a truthful evaluation of the long-time stability of solar cells it is necessary to use a light source that resembles solar AM1.5G conditions.

Stabilizing organic-inorganic perovskite solar cells is a key issue for a successful commercialization. However, so far the degradation mechanisms in general and light-induced processes in particular are still not completely unraveled. In the following sections, we provide a comprehensive overview of a number of degradation mechanisms comprising the effects of moisture, heat, oxygen, light, and high-energy particles. Insights to the degradations and the governing microscopic mechanisms will be given.

3. Perovskite Degradation

3.1. Moisture Induced Degradation

Typical organic-inorganic perovskites – such as $MAPbI_3$ – are strongly hydroscopic. As a result, the material degrades quickly in ambient environment. The process of course can be inhibited by proper device encapsulation and/or by hydrophobic contact or barrier layers.[73,84,97,99,103,104,107,109,112,120,121,126,131,135,145,149] Nevertheless, the underlying mechanism is of general interest. **Figure 2** depicts the general degradation route. The hydration of CH_3NH_3I and PbI terminated surfaces is exothermic. [74] Therefore, solvation as well as water incorporation can be quite swift. Interestingly, a water molecule can reside within the perovskite cavity stabilized by hydrogen bonds to methylammonium and iodine. [74] Recently, the formed hemihydrate $CH_3NH_3PbI_3 \bullet ½H_2O$ has been identified by a subtle shift of the N-H stretching vibrations using Fourier transform infrared spectroscopy (FT-IR). [76]

Concomitantly, O-H stretching vibrations emerge around 3400 cm^{-1}, as shown in figure 2e. [76] The hemihydrate preserves the original crystal structure with minor changes in bond length and a subtle increase of the band gap energy.[74] Although the hemihydrate formation is reversible, two distinct defect states are created.[80] Figure 2f depicts temperature stimulated current (TSC) measurements before and after the formation of the hemihydrate by exposure to humid air.[80] The observed defect states reside in the band gap at energies of 0.32 and 0.42 eV. However, it is unclear whether the energies are given with respect to the valence or conduction band. In addition, hemihydration is accompanied by a strong increase in conductivity.[76]

Upon further exposure to water vapor the monohydrate ($CH_3NH_3PbI_3 \bullet H_2O$) is formed. As a result, the short circuit current J_{SC} is reduced dramatically.[70,78] In contrast to the perovskite and the hemihydrate, the color of the monohydrate is pale yellow. Figure 2b depicts a sketch of the crystal structure determined from X-ray diffraction (XRD).[70,78] The formation of the monohydrate is reversible upon dehydrating. In fact, the short circuit current and the external quantum efficiency (EQE) of TiO_2/$MAPbI_3$/spiro-OMeTAD [2,2',7,7'-tetrakis(N,N-di-p-methoxyphenylamine)-9,9'-spirobifluorene] solar cells recovers completely, as depicted in figure 2g.[78] Note that prolonged exposure to H_2O subsequently leads to the formation of the colorless dihydrate $(CH_3NH_3)_4PbI_6 \bullet 2H_2O$. The corresponding crystal structure is sketched in figure 2c.[78] Due to the loss of CH_3NH_3I, the reaction becomes irreversible. In case of further excess of water, the reaction is finally driven to PbI_2 under expulsion of CH_3NH_3I, figure 2d. [75–78,80,83,86]

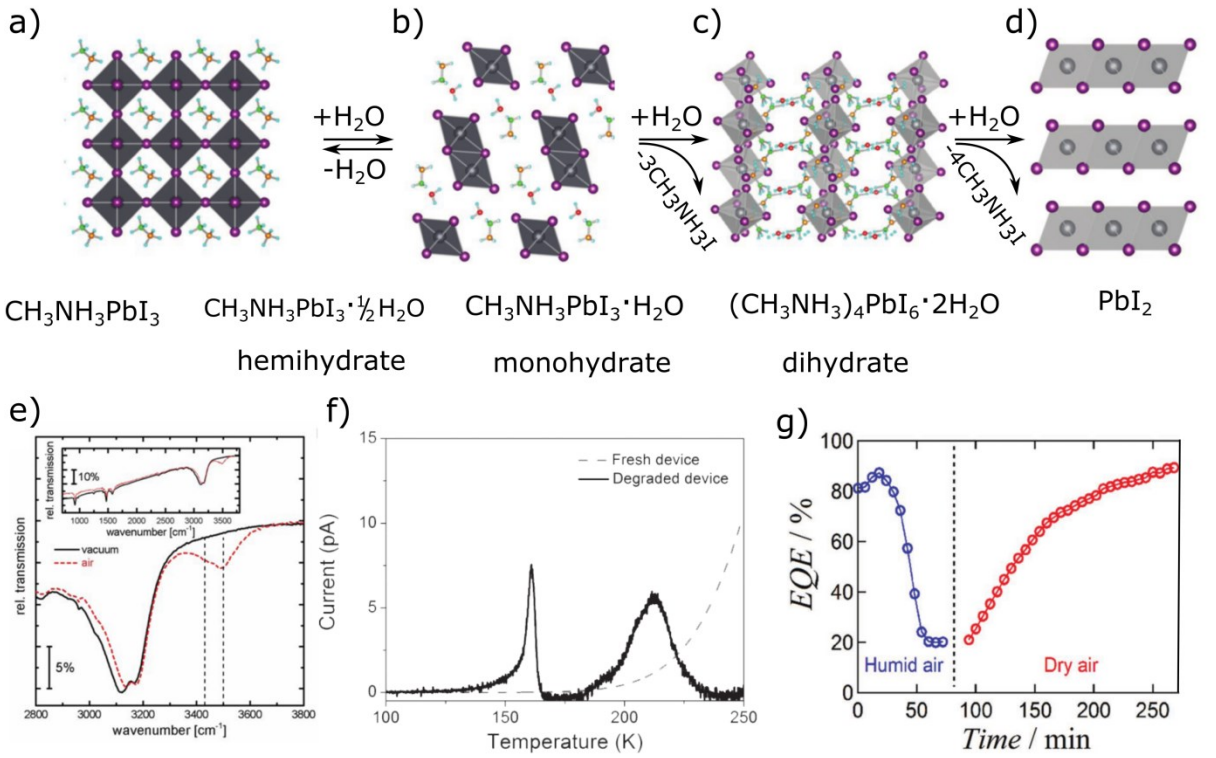

Figure 2. Moisture induced degradation of $MAPbI_3$. (a), (b), (c), and (d) depict the crystal structure of $MAPbI_3$, the monohydrate $CH_3NH_3PbI_3 \cdot H_2O$, the dihydrate $(CH_3NH_3)_4PbI_6 \cdot 2H_2O$, and lead iodide, respectively. Reproduced with permission. [78] Copyright 2016, John Wiley and Sons. (e) FT-IR spectra of $MAPbI_3$ after exposure to vacuum or air. Reproduced with permission. [76] Copyright 2015, American Chemical Society. (f) TSC measurements of freshly prepared and degraded $MAPbI_3$ based solar cells. Reproduced with permission. .[80] Copyright 2015, John Wiley and Sons. (g) External quantum efficiency as a function of exposure time to humid or dry air. Reproduced with permission. [78] Copyright 2016, John Wiley and Sons

In contrast to the observed degradation, small amounts of water added to the precursor solution can induce a controlled and oriented crystallization of $MAPbI_3$. As result, charge carrier lifetimes and power conversion efficiencies are enhanced.[72] Furthermore, impedance spectroscopy and photoluminescence (PL) lifetimes suggest that adsorbed water molecules can effectively suppress certain recombination processes. [79]

3.2. Thermal Instabilities

In thermal equilibrium the temperature of a solar cell is given by [150]

$$T_s = \left[T_0^4 + \frac{1-\eta}{2 \cdot \sigma_s} \cdot P_{sun}\right]^{1/4} \quad (1)$$

Neglecting convection, T_S is determined by the Boltzmann constant, σ_S, the efficiency, η, the integrated power of the solar spectrum, P_{sun}, and the temperature of the environment, T_0. For a solar cell with an efficiency of $\eta = 20$ % and an outdoor temperature of $T_0 = 45$°C (typical

summer conditions), T_S amounts to about 83 °C. Hence, under typical environmental conditions a solar cell needs to withstand this temperature.

In general, perovskites undergo phase transitions depending on the temperature. As an example, $MAPbI_3$ exhibits two phase transitions. The first one occurs at about 160 K when its phase changes from orthorhombic (Pnma) to tetragonal (I4/mcm). A second phase transition from tetragonal to cubic (Pm3m) is observed at about 330 K.[151,152] The corresponding crystal structures are depicted in **Figure 3**a.[152] The band gap energy decreases with increasing temperature for a given crystalline structure and shows an abrupt change at the phase transition (see figure 3b). The high temperature phase transition is of particular interest, since it resides within the operating temperatures of a solar cell. On the other hand, the photovoltaic properties do not change abruptly at the phase transition. [153–155] Instead, J_{SC} and V_{OC} decrease monotonically, as shown in figure 3c. The lack of an abrupt change is attributed to the high structural flexibility in the high temperature phase.[154] Since the temperature of solar cells can vary from night to day between about – 40 °C and 85 °C the influence of temperature cycling and phase transitions on the long-term stability are of importance. However, such experiments have not been performed to date.[156] Note that commercial absorber materials, such as crystalline/amorphous Si, $Cu(In,Ga)Se_2$, CdTe, GaInAs, GaInP or Ge do not have phase transitions in this temperature range.

Besides structural changes, organic-inorganic perovskites - especially $MAPbI_3$ - degrade at elevated temperatures. Interestingly, investigations on the temperature stability differ vastly depending on the used technique. On the one hand, thermogravimetric analyses (TGA), as presented in figure 3d, often reveals a thermal stability exceeding T = 250 °C. [1,60] On the other hand, numerous other experimental techniques show that $MAPbI_3$ degrades already at lower temperatures. For instance, XRD shows the reflex of the (001) plane of hexagonal PbI_2 ($2\Theta \approx 12.6°$) already at temperatures above 140 °C (figure 3e). [65] At the same temperature, the reflex originating from the (110) plane of tetragonal $MAPbI_3$ ($2\Theta \approx 14.1°$) vanishes and at T > 190°C the decomposition of $MAPbI_3$ to PbI_2 is completed.

Wavelength dependent surface photovoltage (SPV) measurements taken after heating give further insight into the altered charge separation processes (figure 3f).[66] Up to a temperature of 140 °C the material quality increases since the charge separation by defect states within the band gap is reduced. Above 140°C charge separation by defect states increases due to an additional photovoltage located at about 2.4 eV. This behavior corresponds to charge separation in PbI_2, which is formed due to thermal degradation.

Conversely, a temperature of 85°C seems high enough to degrade the surface of $MAPbI_3$ films. As an example, figure 3g depicts X-ray photoelectron spectroscopy (XPS) measurements of $MAPbI_3$ films before and after annealing at 85°C in various atmospheres. [62] In pristine samples, the C1s core level is dominated by a peak representing the C-N bond of methylamine. Upon prolonged annealing at 85°C in ambient air, pure O_2, or pure N_2 the C-N related peak decreases gradually and the peak related to C-C or C-H bonds increases. The observed surface degradation is sufficient to affect the performance of $TiO_2/MAPbI_3$/P3HT [poly(3-hexylthiophen-2,5-diyl] devices. In particular, FF and J_{SC} decrease by about 50 % during an anneal at 85°C for 24 hrs in ambient atmosphere. [62]

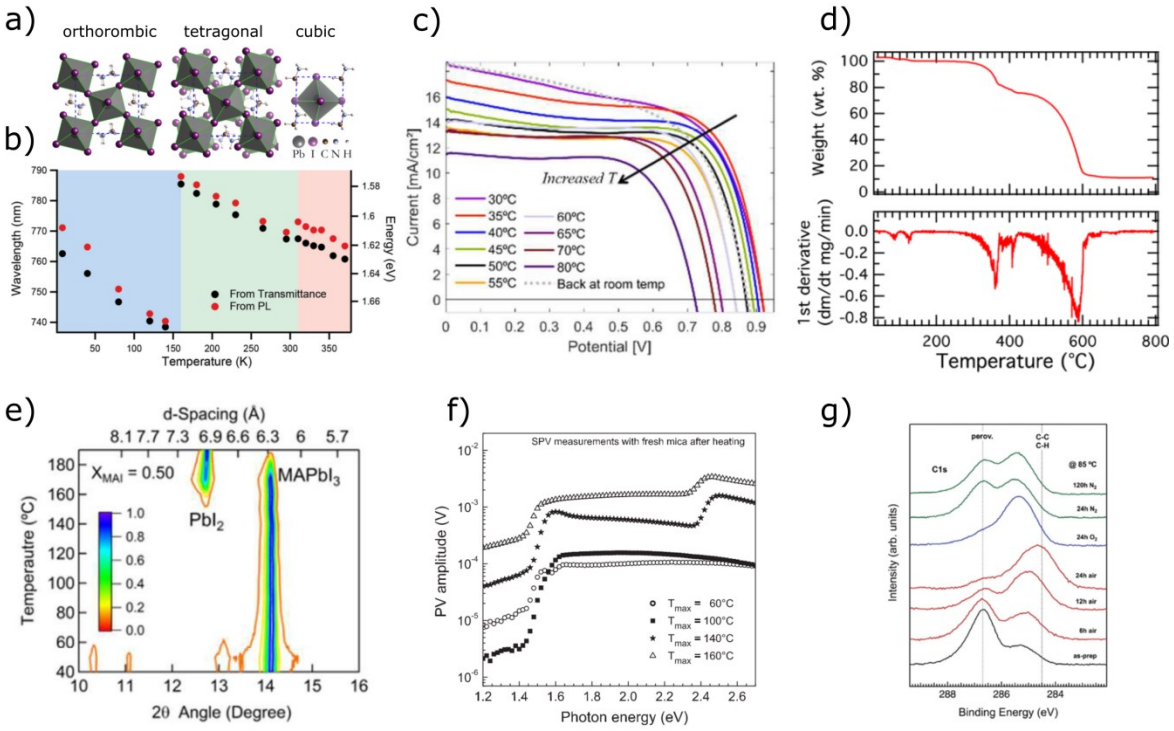

Figure 3. Heat induced degradation of $MAPbI_3$. (a) Schematic representation of the $MAPbI_3$ crystal structures. Reproduced with permission. [152] Copyright 2015, American Physical Society. (b) Temperature dependent band-gap position of $MAPbI_3$. Reproduced with permission. [157] Copyright 2015, John Wiley and Sons. (c) Temperature dependent *J*-V characteristics of a regular $TiO_2/MAPbI_3$/spiro-OMeTAD solar cell. Reproduced with permission. [155] Copyright 2016, American Chemical Society. (d) TGA heating curves of $MAPbI_3$. Reproduced with permission. [60] Copyright 2014, American Chemical Society. (e) X-ray diffractogram of $MAPbI_3$ as a function of temperature. Reproduced with permission. [65] Copyright 2015, American Chemical Society. (f) SPV measurements of $MAPbI_3$ layers after annealing at moderate temperatures. Reproduced with permission. [66] Copyright 2013, American Institute of Physics. (g) XPS measurements of $ITO/TiO_2/MAPbI_3$ samples at 85°C in various indicated atmospheres. Reproduced with permission. [62] Copyright 2015, John Wiley and Sons.

Compositional engineering allows to strengthen the thermal stability of perovskites. For instance, a replacement of the methylammonium cations with Cs^+ or formamidinium cations, $HC(NH_2)_2^+$, is possible. Cesium lead halides are stable up to temperatures of 300°C.[158,159] Formamidinium (FA) lead halides are stable up to temperatures of at least 200°C. **Figure 4**a depicts an X-ray diffractogram of $FAPbI_3$ in the α-phase, acquired at a temperature of 170°C. Notably, reflexes originating from hexagonal PbI_2 are absent. This suggests a higher thermal stability than observed for $MAPbI_3$. However, when pure $FAPbI_3$ is cooled to room temperature the perovskite undergoes a phase transition to a hexagonal structure (δ-phase). This phase is yellow and therefore not suitable for solar cells.[160] This structural transformation can be suppressed by blending formamidinium with methylammonium. [160,161] Even more complex blends, comprising rubidium, cesium, formamidinium, and methylammonium, have been explored recently. [41,42] These triple or quadruple mixed cation perovskites exhibit high power conversion efficiencies and a superior thermal stability compared to perovskites prepared with pure methylammonium cations. As an example, figure 4b shows the evolution of the power conversion efficiency of a $Rb_5(Cs_5MA,FA)_{95}Pb(_{1.83}Br_{0.17})_3$ based solar cell. Although the device is exposed to a temperature of 85°C and continuous illumination with a power density of 100 $mWcm^{-2}$ the degradation is less than 5 % over a period of 500 hrs. [41] Note that detailed investigations on heating induced defects in triple or quadruple cation perovskites have not been performed to date.

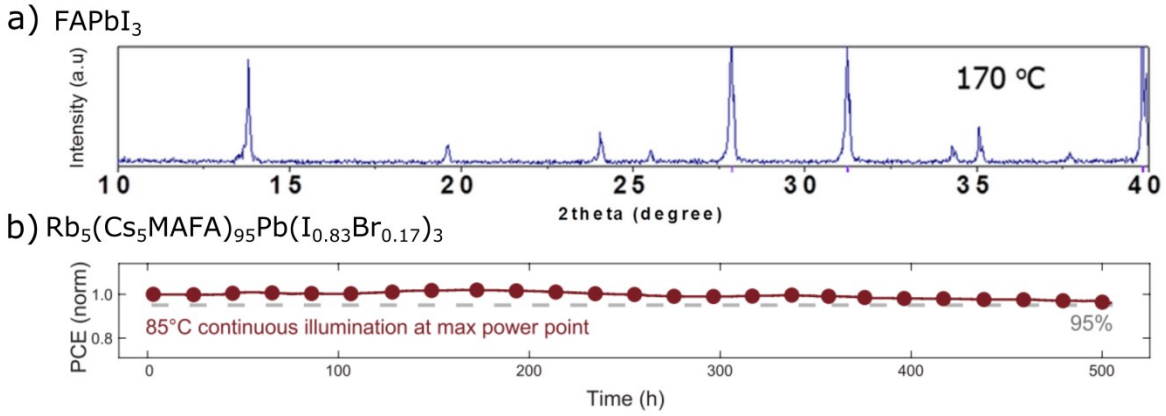

Figure 4. Thermal stability of FA based perovskites. (a) X-ray diffractogram of $FAPbI_3$ measured at 170°C. Reproduced with permission. [161] Copyright 2015, Nature Publishing Group. (b) Power conversion efficiency of a $Rb_5(Cs_5MA,FA)_{95}Pb(_{1.83}Br_{0.17})_3$ based solar cell as a function of time. The measurements were performed at a temperature of 85°C. The device was continuously illuminated with a light intensity of 100 $mWcm^{-2}$ using white LEDs. Reproduced with permission. [41] Copyright 2017, The American Association for the Advancement of Science.

3.3. Photo-Induced Degradation

Comparing T_{80} lifetimes of over 50 publications, we revealed a considerably reduced lifetime of perovskite solar cells under illumination (see figure 1, chapter 2). Most notably, the sun spectrum contains a considerable amount of high energetic photons, which are particularly harmful to perovskite solar cells.[139,148] Since solar cells need to be optimized for maximal absorption of a broad spectral range, this is highly problematic. With only a few publications so far, the investigation of photo-induced degradation is still in its infancy. In the following, we critically review recently observed light-induced degradation mechanisms. First, we focus on the interaction of oxygen and light, which results in a swift degradation. [54,58,77] However, photo-induced degradation does not require the presence of oxygen. Therefore, we will discuss a number of reversible[57,162,163] and unfortunately also permanent[148,162,164] degradation processes reported throughout literature. In particular, we will highlight the observed dissociation of $CH_3NH_3^+$, which commences under illumination with $h\nu \geq 2.72$ eV.[148] Beyond that, mixed cation and mixed halide perovskites are prone to phase segregation under illumination.

3.3.1. Oxygen Catalyzed Photo-Degradation

Mesoporous (mp) TiO_2 sensitized solar cells are susceptible to rapid degradation by ultra-violet light. This effect is a result of oxygen desorption, which activates oxygen vacancies within TiO_2. These act as deep electronic trap states [165] and finally quench the performance of perovskite and dye sensitized solar cells. [139,144]

However, even in the absence of mp-TiO_2 and/or UV-light, the combined action of molecular oxygen and light induces a rapid degradation of organic-inorganic perovskites. [54,58,166] **Figure 5**a depicts absorption spectra of $MAPbI_3$ on glass prior to and after aging in dry air under illumination. [58] After a course of 48 hours, the absorption onset clearly shifts from around 800 nm to 500 nm. This corresponds to a complete degradation to PbI_2. It should be noted, that in absence of O_2 or light, no degradation was observed. [58] This effect was confirmed by measuring the efficiency of FTO/cp-TiO_2/mp-TiO_2/$MAPbI_3$/spiro-OMeTAD/Au based devices in various atmospheres, see figure 5b. [58] Again, no degradation is observed in absence of O_2 or light. Note that a UV filter was used to prevent the activation of TiO_2 related defects.

The mechanism of the combined oxygen and light induced degradation is currently under debate. [54,56,58,148] Super-resolution luminescence micro-spectroscopy, for example, revealed a smooth collapse of the $MAPbI_3$ crystal structure to PbI_2, starting locally and then spreading over the whole crystal. [56] Further, hydroethidine was used recently as a molecular fluorescent probe.[54] The molecule has a characteristic emission upon exposure to the superoxide (O_2^-). Perovskite films that were immersed in the probe solution caused an increase of the characteristic emission when illuminated.[54] This shows that O_2^- triggers the degradation under combined O_2 and light exposure. As the governing mechanism, it was suggested that illumination leads to the formation of the superoxide, which subsequently causes the deprotonation of $MAPbI_3$ and the formation of methylamine, lead iodide, iodine, and water as byproducts. [54]

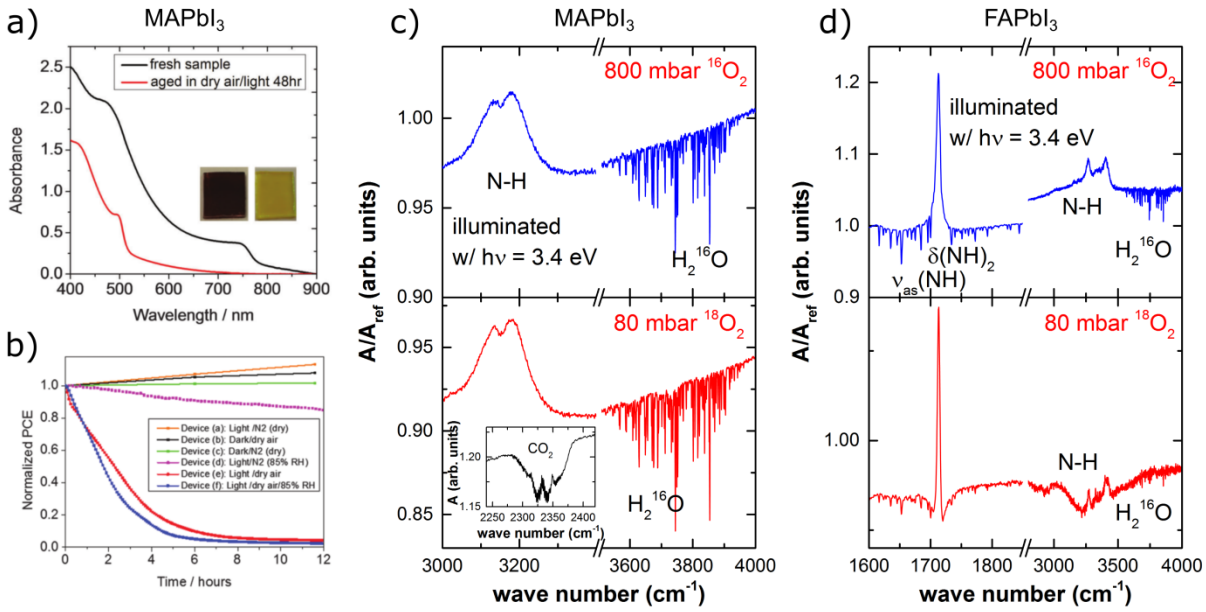

Figure 5. Oxygen catalyzed photo-degradation of perovskites: (a) Absorption spectra of $MAPbI_3$ on glass prior to and after prolonged illumination. (b) Evolution of the normalized η of FTO/cp-TiO_2/mp-TiO_2/$MAPbI_3$/spiro-OMeTAD/Au devices in various environments. Illumination was performed with white LEDs that were equipped with a UV filter. (a,b) Reproduced with permission. [58] Copyright 2016, The Royal Society of Chemistry. (c), (d) FT-IR spectra of $MAPbI_3$ that were exposed to UV light and isotopically enriched $^{16}O_2$ or $^{18}O_2$. The inset shows the absorption modes of $C^{16}O_2$ and $C^{18}O_2$. Reproduced with permission. [148] Copyright 2017, unpublished. (d) FT-IR spectra of $FAPbI_3$ after exposure to UV light and $^{16}O_2$ or $^{18}O_2$. (c,d) The FT-IR spectra were normalized to the spectra of untreated pristine perovskites.

The light-induced degradation in the presence of oxygen was revisited to elucidate the exact microscopic mechanism. Before and after light exposure in the presence of oxygen the samples were characterized using FT-IR measurements. For these experiments isotopically

enriched $^{16}O_2$ and $^{18}O_2$ was used. Figure 5c depicts the absorption ratio of the illuminated to the pristine unexposed sample, A/A_{ref} for $FAPbI_3$. It is important to note that an increase of the absorption ratio corresponds to a decrease of the corresponding molecular concentration. On the other hand, the absorption lines for water point downward. Since the unexposed sample (A_{ref}) did not show H_2O vibrational modes, their appearance indicates that water molecules escaped from the sample into the airtight sample compartment. The upper panel of figure 5c depicts the infrared absorption after an UV degradation in the presence of $^{16}O_2$ (800 mbar). The photon energy, photon flux, and degradation time amounted to $h\nu = 3.4$ eV, photon flux $F \approx 5\times10^{17}$ $s^{-1}cm^{-2}$, and $t = 4.5\times10^3$ s, respectively. The two asymmetric N-H stretching modes are located around 3130 and 3178 cm^{-1}.[167] Clearly, the NH_3^+ concentration in the perovskite sample is strongly reduced after the degradation. This is consistent with the dissociation of $CH_3NH_3^+$ and the out-diffusion of the degradation products. Simultaneously, absorption lines of water vapor, pointing downwards, emerge. These H_2O molecules evolved from the $MAPbI_3$ thin films. Previously, it was suggested that H_2O forms from oxygen that diffuses into the specimens and protons from the organic cations. [54,58] To test this hypothesis the degradation experiment was repeated in the presence of isotopically enriched $^{18}O_2$ (80 mbar). If the light-induced degradation results in the formation of water molecules one would expect to observe vibrational modes of $H_2{}^{18}O$, that are shifted in frequency due to the heavier ^{18}O atoms. However, the IR spectra do not show an isotope shift of the water lines (figure 5c lower panel). Hence, this experiment demonstrates that water is *not* a reaction product of the light-induced degradation process. Instead, perovskite samples already contain H_2O, most likely in form of crystallization water. [72,74,79] To show that the atmosphere did contain ^{18}O the vibrational modes of CO_2 are depicted in the inset. The modes consist of $C^{16}O_2$ and $C^{18}O_2$. Hence, the data presented in figure 5c clearly demonstrate that oxygen acts as a catalyst only.

Molecular oxygen is known to diffuse within $MAPbI_3$. [168] Its charge state resides about 0.2 eV below the conduction band of $MAPbI_3$. [169] Under charge injection or illumination with $h\nu \geq E_G$, free charge carriers are generated within $MAPbI_3$.[170] Consequently, an O_2 molecule can capture a free electron from the conduction band, forming superoxide in the $^2\Pi_g$ configuration (equation 2). The O_2^- and $CH_3NH_3^+$ ions are a Brønsted-Lowry base and acid, respectively. Therefore, in a further reaction step $CH_3NH_3^+$ is deprotonated (see equation 3). The produced methylamine diffuses out of the sample and hence, impedes any back-reaction.

In a final step, the produced HO_2 molecules dissociate into molecular hydrogen and oxygen and the H_2 molecules diffuse out of the sample. Then, the remaining O_2 molecules can act as catalyst for the next dissociation process (equation 4).

$$O_2 \xrightarrow[\mathrm{MAPbI_3}]{h\nu \geq E_G} O_2^- \quad (2)$$

$$CH_3NH_3^+ + O_2^- \longrightarrow HO_2 + CH_3NH_2 \uparrow \quad (3)$$

$$2\ HO_2 \longrightarrow 2O_2 + H_2 \uparrow \quad (4)$$

So far, studies have been limited to $MAPbI_3$.[54,58,77,148] However, most recent perovskite solar cells utilize complex blends of methylammonium and formamidinium together with small inorganic cations.[41,42,81,171] Therefore, we present for the first time FR-IR spectra of polycrystalline $FAPbI_3$ after light-induced degradation in oxygen atmosphere (figure 5d). Most notably, the dissociation of $HC(NH_2)_2^+$ is equally swift as for $CH_3NH_3^+$. The upper panel in figure 5d depicts measurements recorded after the exposure to $^{16}O_2$ (800 mbar) and ultra violet light ($h\nu$ = 3.4 eV, photon flux $F \approx 5\times10^{17}$ $s^{-1}cm^{-2}$ for 3.6×10^3 s). The stretching vibration of the N-C bond and the N-H bending vibrations are located near 1700 cm^{-1}. The N-H stretching vibrations are located between 3200 and 3500 cm^{-1}. After the degradation the N-H and C-N related absorption modes are reduced considerably. This is consistent with the dissociation of $HC(NH_2)_2^+$. At the same time an increase of H_2O absorption lines is observed. The same degradation experiment was performed with isotopically enriched $^{18}O_2$ (80 mbar) and the spectra are shown in the lower panel of figure 5d. As for $MAPbI_3$, an isotopic shift of the water lines is not observed, which clearly shows that H_2O is *not* formed from the supplied $^{18}O_2$ molecules. As a matter of fact, independent of the organic cation, oxygen merely serves as a catalyst for the deprotonation of the cation. Hence, the microscopic degradation mechanism is similar to the one proposed for $MAPbI_3$, but differs for the individual reactions and the final byproducts that are formed. $HC(NH_2)_2^+$ is deprotonated forming imidoformamide, which subsequently diffuses out of the host lattice. This is consistent with the observed loss of C-N and N-H reflected by a gain of the A/A_{ref} ratio (see figure 5d).

For the low oxygen pressures (80 mbar, lower panel), additional absorption lines around ~1711 cm^{-1}, ~2900 cm^{-1}, and ~3200 cm^{-1} emerge after degradation. Note that the absorption lines point downward because the FT-IR spectrum of the unexposed specimen did not contain

these vibrational modes. It is conceivable that imidoformamide further dissociates into fragments causing the rise of these new absorption lines.[172] For high oxygen pressures (800 mbar) the loss of $HC(NH_2)_2^+$ related C-N and N-H modes is dominant. A reliable identification of the produced imidoformamide fragments requires further experiments and will be published at a later date.

3.3.2. Photo-dissociation

Several groups observed significant photo-instabilities of $MAPbI_3$.[56,57,59,164,173–177] However, most experiments were performed in air. Thus, the dominant degradation mechanism is a consequence of the combined action of oxygen and light. A few groups studied the effect of light soaking of $MAPbI_3$ in inert atmosphere. Astonishingly, a strong increase in photoluminescence intensity[168,177,178] , open circuit voltage, and short circuit current [179] was shown. As result, power conversion efficiencies often increase within the first seconds to minutes upon illumination. [57,179,163] Recently, this so called *photo-curing* behavior has been associated with a reduction of the density of trapping sites from initially $\approx 10^{17}$ cm^{-3} to about 10^{16} cm^{-3}. [178] It was suggested that illumination annihilates iodine vacancy/interstitial Frenkel pairs. [178] These defects are relatively common in $MAPbI_3$ and are shown to diffuse easily.[178,180] Huang et al.[163] further proved that the positive effect of photo curing-vanishes upon storage in the dark. In fact, the efficiency η decreases to less than 10 % of the maximal value after 12 hours in darkness. Upon light exposure, the efficiency subsequently recovers repeatedly. Interestingly, a photo-induced degradation was not observed in this study.

Conversely, several other groups report on the commencement of a photo-induced degradation after several minutes of illumination [57,162,173], as shown in **figure 6**a. [57] Within the first minutes of illumination, the authors observe an increase in η. Then however, light-induced degradation commences. When the solar cells are kept at $V = V_{OC}$ (condition A) Nie et al. [57] show a 30 % degradation over the course of 2 hrs under illumination. Near infrared absorption indicates the formation of deep trapping levels. [57] Interestingly, the degradation decelerates when the devices are operated at V = 0 V (condition B). The solar cells recover in the dark, as the majority of trapping states dissipates. This recovery is strongly temperature dependent. Figure 6b depicts the degradation and self-healing scheme. Within a microscopic picture, it is suggested that localized polarons form upon illumination. They reside deep within the band gap and act as trapping states. The corresponding structural distortions are

corroborated by DFT calculations [57] and an increase of distinct Raman modes [57,181]. A deeper insight into the governing mechanism can be found elsewhere. [57]

Domanski et al. [162] observed a very similar photo-induced degradation while operating devices at the maximum power point. This is depicted in figure 6c. In general, they differentiate two distinct degradation mechanisms: a swift degradation within the first hours and a somewhat slower mechanism. They show that the fast degradation process is fully reversible upon storing devices in the dark. This is identical to the study by Nie et al.[57] (figure 6a). Conversely, Domanski et al. [162] attribute the effect to the migration of ionic vacancies. As depicted in figure 6d, they suggest an initially random distribution of anion and cation vacancies, which migrate and form Debye layers at the charge selective contacts under working conditions. This induces reversible performance losses. In general, ion migration is widely accepted in organic-inorganic perovskites. [182] Activation energies for migration are in the range of 0.1 to 0.8 eV in $MAPbI_3$. [174] This is a low value range even compared to oxide ion conductors used in fuel cell, such as $LaFeO_3$ where typical activation energies are reported in the range of 0.5 to 2 eV [183]. The migration of ions or ionic defects is believed to be responsible for slow photoconductivity responses [174], solar cell hysteresis [184] or switchable photocurrents. [67] A detailed report on ion migration in $MAPbI_3$ can be found elsewhere. [182] It must be noted, however, that Domanski et al. [162] investigated a mixed cation, mixed halide $(FAPbI_3)_x(MAPbBr_3)_y$ perovskite. Such alloyed perovskites are prone to photo-induced phase segregation, which might affect the reported results. This behavior is discussed in more detail in section 3.3.3.

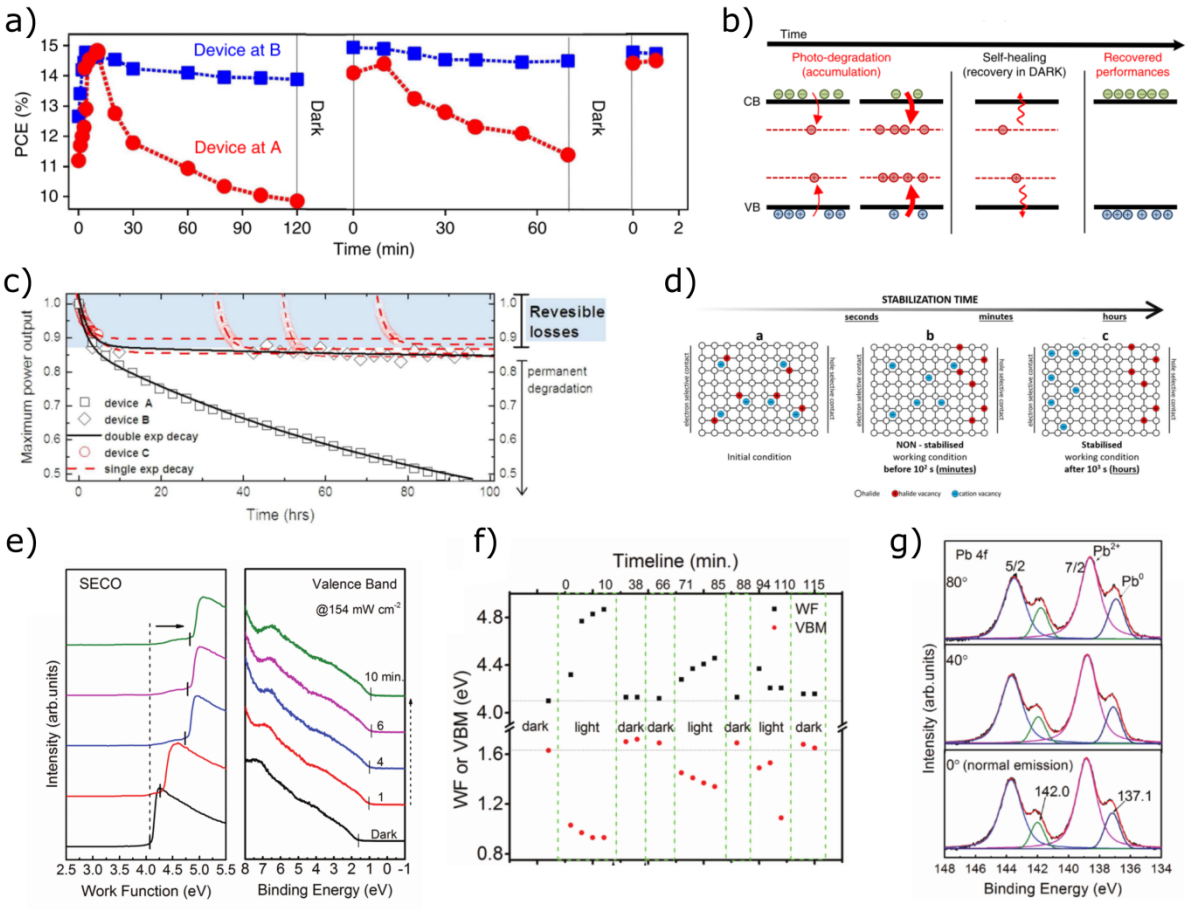

Figure 6. Photo degradation of organic-inorganic perovskites: (a) Power conversion efficiency of ITO/PEDOT:PSS/$MAPbI_3$/PCBM/Al devices under constant illumination. Devices were stressed either at $J = 0$ and $V = V_{OC}$ (condition A) or $J = J_{SC}$, $V = 0$ (condition B). (b) Proposed mechanism of photo-degradation and self-healing processes. (a, b) Reproduced with permission. [57] Copyright 2016, Nature
(c) Maximum power-point tracking of FTO/TiO_2/mp-TiO_2/$(FAPbI_3)_x(MAPbBr_3)_y$/spiro-OMeTAD/Au devices under continuous UV filtered LED illumination. Devices A and B were continuously tracked, while device C was cyclically tracked for 5 hours and then stored in the dark. (d) Schematic depiction of the evolution of the ion distribution within the perovskite layer. (c, d) Reproduced with permission. [162] Copyright 2017, Wiley. (e) Time dependent UPS spectra of $MAPbI_{3-x}Cl_x$ thin films under white LED illumination (154 mW cm^{-2}) (f) Evolution of the work function and VBM over multiple on-off illumination cycles. (g) Angle dependent XPS spectra of the thin film after multiple on-off illumination cycles. (e, f, g) Reproduced with permission. [164] Copyright 2016, Wiley.

As indicated before, Domanski et al. observed a second somewhat slower mechanism, which leads to permanent degradation. As the kinetics of the slow process vary vastly between identically prepared devices (device A & B in figure 6c), they propose that one or more device components are involved.

Recently, Zu et al. [164] observed permanent degradation on $MAPbI_{3-x}Cl_x$ films and $MAPbI_3$ single crystals. They perform ultraviolet photoelectron spectroscopy (UPS) measurements

prior to, during, and after exposure to white light. A gradual shift of the valence band maximum (VBM) and the work function due to surface photovoltage under illumination was reported (see figure 6e). For low photon doses, these shifts are, as expected, reversible. However, for high photon doses of about 154 Wcm^{-2} and long-term illumination the surface photovoltage vanishes. Using angle dependent XPS they identify the formation of $Pb^{(0)}$ after intense prolonged illumination. The authors suggested that the formed $Pb^{(0)}$ induces a strong pinning of the Fermi energy close to the conduction band maximum. Simultaneously, a different absorption was observed that was attributed to PbI_2, which formed during the illumination in high vacuum.

It appears that light induced degradation of $MAPbI_3$ based solar cells involves two distinct processes: a swift but reversible degradation process and a slower degradation process that causes irreversible changes of the samples. The latter irreversible degradation process has not been subject to investigations so far. To elucidate the irreversible degradation of organic inorganic perovskites we performed light-induced gas-effusion experiments. [148] For this purpose polycrystalline $MAPbI_3$ thin films were placed into a gas effusion setup with a base-pressure of 10^{-8} mbar. The residual gas composition was measured as a function of time using a quadrupole mass spectrometer. Figure 7a depicts the ion current as a function of time for H_2, HD, CH_2, NH_2, CH_3NH_2, and CH_3NH_3; D represents the hydrogen isotope deuterium (^2H). Without illumination, the ion currents are constant. After 6200 s a blue LED with an excitation energy of $h\nu = 2.72$ eV and a photon flux of $F \approx 3\times10^{17}$ $s^{-1}cm^{-2}$ is switched on (see red arrow). After a short delay of about 200 s the ion currents of all monitored masses increase. It has to be noted, that all masses reach a maximum ion current at $t \approx 7860$ s except for CH_3NH_3, which exhibits its maximum ion current already at $t \approx 6880$ s. Light-induced gas effusion experiments were repeated using an ultraviolet LED ($h\nu = 3.4$ eV, $F \approx 5\times10^{17}$ $s^{-1}cm^{-2}$) and a red LED ($h\nu = 3.4$ eV, $F \approx 5\times10^{17}$ $s^{-1}cm^{-2}$). The obtained results are shown in figures 7b and 7c. For clarity ion currents for HD, CH_2, and NH_2 are omitted. Their time dependence is the same as for the other molecules.

When illuminating with UV or blue light all ion currents increase. However, in case of red light the ion currents do not increase with time. Hence, the excitation energy for the light induced degradation of $MAPbI_3$ has to be equal to or exceed 2.72 eV. The observation of H_2 and HD out-diffusion from the perovskite layer upon illumination implies that N – H/D bonds dissociate. Further insight into the microscopic mechanism can be obtained from the onset of

the ion current traces. In particular, the ion current for CH_3NH_3, increases first and decreases to its background value before H_2 and CH_3NH_3 reach their maximum. It is likely that out-diffusion of CH_3NH_3 is limited to a small amount that originates from a surface near region.[148] The subsequent increase of the ion currents for H_2, HD, and CH_3NH_2 molecules implies that illumination results in the deprotonation of CH_3NH_3 in the perovskite lattice.

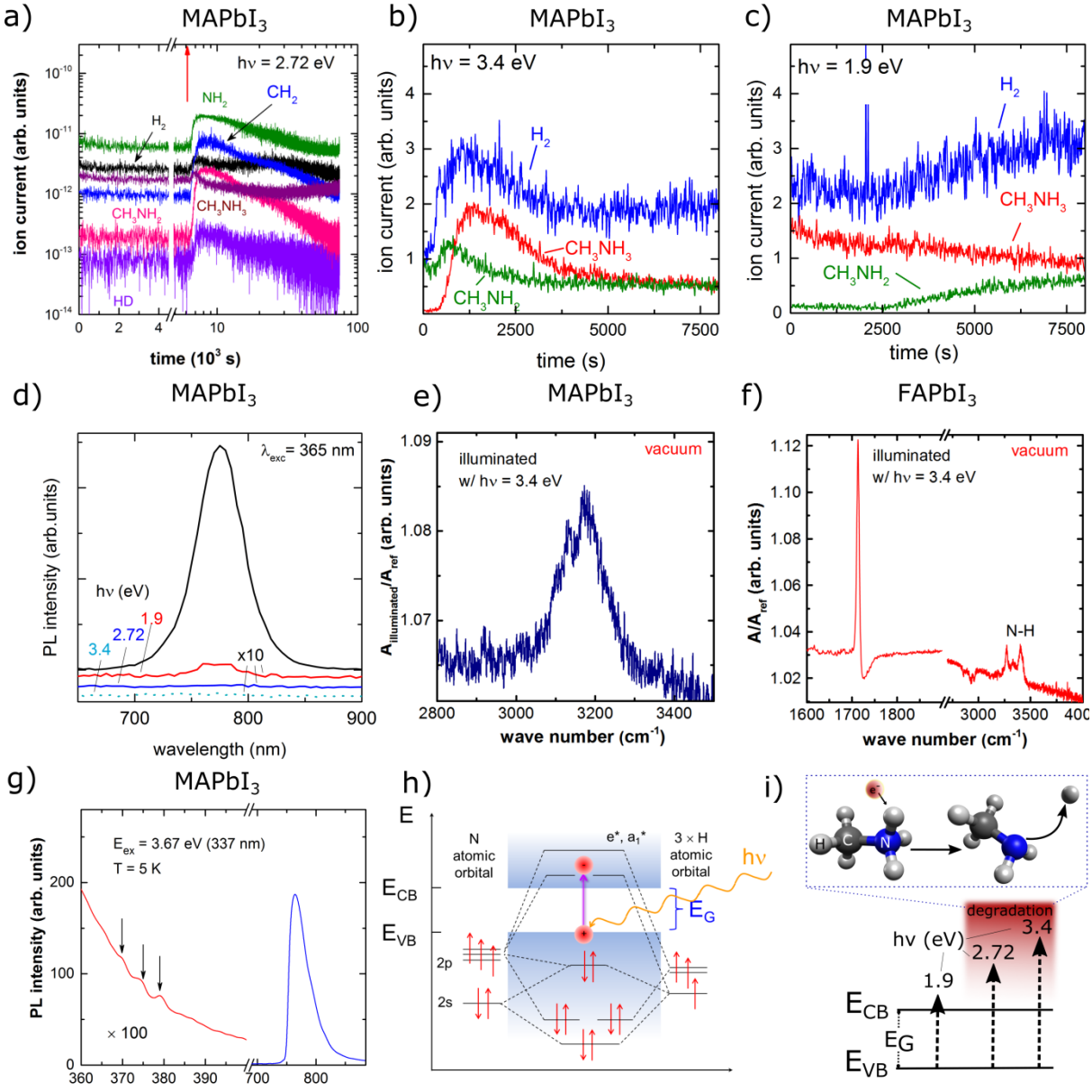

Figure 7. Light-induced dissociation of organic-inorganic perovskites. (a) Ion current of H_2, HD, CH_2, NH_2, CH_3NH_2, and CH_3NH_3 as a function of time. At t = 6200s the $MAPbI_3$ sample was illuminated with $h\nu$ = 2.72 eV and a photon flux F ≈ 3×10^{17} $s^{-1}cm^{-2}$. (b) Ion current as a function of time under illumination with UV light; $h\nu$ = 3.4 eV, F ≈ 5×10^{17} $s^{-1}cm^{-2}$. (c) Ion current as a function of time under illumination with red light; $h\nu$ = 1.9 eV, F ≈ 5×10^{17} s. (d) Photoluminescence spectra of $MAPbI_3$ samples before (black curve) and after illumination for about $t = 7.4\times10^4$ s with a photon energy of $h\nu$ = 1.9 eV (red curve), 2.72 eV (blue curve), and 3.4 eV (dashed curve). (e) FT-IR spectra of $MAPbI_3$ after exposure to UV light ($h\nu$ = 3.4 eV, $t_{ill} = 2.82\times10^4$ s) in vacuum. The data are normalized to the untreated specimen prior to

illumination. (f) FT-IR spectra of $FAPbI_3$ after exposure to UV light ($h\nu$ = 3.4 eV, t_{ill} = 2.82×10^4 s) in vacuum. The data are normalized to the untreated specimen prior to illumination. (g) Photoluminescence spectra of $MAPbI_3$ samples recorded at T = 5 K. The ultraviolet part of the photoluminescence spectrum is magnified by a factor of 100. (h) Schematic depiction of the molecular orbitals of ammonia in respect to the perovskite conduction and valence bands. (i) Schematic depiction of the dissociation mechanism of $CH_3NH_3^+$ due to the capture of a photo-generated electron. (a, d, g, and h) Reproduced with permission. [148] Copyright 2017, John Wiley and Sons.

The proposed photo-induced deprotonation was corroborated using FT-IR measurements before, during, and after illumination in vacuum.[148] Figure 7e depicts the ratio of the illuminated to the pristine unexposed sample, A/A_{ref}. The observed change in A/A_{ref} points upwards. This corresponds to a decrease of amine concentration in the lattice after illumination. This is consistent with the light-induced effusion measurements showing that illumination results in the dissociation of N – H bonds. Consequently, the opto-electronic properties of $MAPbI_3$ are deteriorated vastly. Figure 7d depicts PL measurements before and after prolonged illumination. Note, that the yield of the PL intensity is inversely proportional to the concentration of localized defects.[185,186] Already after illumination with $h\nu$ = 1.9 eV for $t = 7.4\times10^4$ s in vacuum, the PL yield decreased significantly. However, as soon as the photon energy exceeds 2.7 eV a vast number of localized defects is created, which results in a complete quenching of the band-to-band photoluminescence. Most likely, the localized defects are fragments of the methylammonium ions that have energy levels in the band gap of the perovskite. [187,188]

Considering the observed photo-dissociation of N – H bonds in $MAPbI_3$ a microscopic mechanism was proposed. [148] Upon illumination with light of $h\nu \geq 2.7$ eV the dissociation of N – H bonds occurs according to the reaction:

$$2(CH_3NH_3^+) + 2\,e^- \rightarrow 2(CH_3NH_2) + H_2 \quad . \qquad (5)$$

This is schematically depicted in figure 7i. In general, photo-dissociation of NH_3 can occur if an electron is placed in one of the antibonding orbitals. Figure 7h illustrates the molecular orbitals of NH_3 according to molecular orbital theory. Most notably, the antibonding molecular orbitals e^* and a_1^*, are high in energy and unoccupied.[148] It is interesting to note, that photo-dissociation of isolated NH_3 requires an energy of around 6.4 eV.[189] This is far beyond the photon energies used above and usually takes place in Jovian's atmosphere only.[190] In the hybrid semiconductor molecular orbitals from $CH_3NH_3^+$ form energy bands which reside deep in the valence and conduction bands. *Ab-initio* methods predicted a minimal energy of 8 eV, which is needed for a direct transition from the valence band

maximum into empty conduction bands associated to $CH_3NH_3^+$. [191,192] In principle such a transition should *not* occur, as excited electrons usually thermalize down to the conduction band-edge within 10^{-11} s. However, it has been shown recently, that the hot carrier lifetime in $MAPbI_3$ is about 3 orders of magnitude higher as compared to conventional semiconductors. [193,194]

Figure 7g shows photoluminescence measurements of $MAPbI_3$ taken at 5 K. In addition to the band gap luminescence at 1.62 eV, Nickel et al [148] observe three hitherto unknown PL peaks located at 3.27, 3.31, and 3.34 eV. It was concluded that these states correspond to the antibonding orbitals of NH_3. As they give rise to luminescence, it is clear that they are *not* in resonance with the conduction bands of the crystal lattice of the $MAPbI_3$. Therefore, the data suggest that the dissociation of $CH_3NH_3^+$ commences by trapping charge in the antibonding states of N – H, which requires a minimal energy of about 2.72 eV.

Reports on photo-dissociation so far have been limited to methylammonium lead iodide. [148] It is, however, conceivable that photo-dissociation occurs also in other organic cations utilized in perovskite solar cells. Formamidinium in particular is the second most utilized cation. [41,42] Hence, similar light-induced degradation experiments were performed on polycrystalline $FAPbI_3$ thin films. Figure 7f depicts the A/A_{ref} ratio calculated from FT-IR measurements before and after exposure to UV light ($h\nu$ = 3.4 eV) in vacuum. Consistent with the dissociation of $HC(NH_2)_2^+$, a vast decrease in absorption associated to N-H and N-C bands is observed. The N-H stretching modes are located between 3200 and 3500 cm^{-1}, while the N-H bending and N-C stretching bonds are located at ≈1700 cm^{-1}. Interestingly, the A/A_{ref} of $FAPbI_3$ contains vibrational bands around 1710 cm^{-1} and 2900 cm^{-1} pointing downwards. These correspond to absorption bands, which were not present in the unexposed specimen. Hence, $HC(NH_2)_2^+$ is not only deprotonated to imidoformamide but also fragmented further within the host lattice upon illumination. For a thorough identification of the dissociation mechanism, additional experiments are required in the future.

Light-induced degradation of perovskites in the absence of O_2, TiO_2, moisture, and heat is broadly discussed in the literature. While not all reported changes of device parameters and materials properties are supported with exact models the data presented in figure 7 establish that deprotonation of the organic cation occurs for photon energies ≥ 2.7 eV. In fact, it is conceivable that even hot carriers with sufficient energy can be trapped by the N-H

antibonding states, which ultimately results in the dissociation of the cation. This seems highly relevant for degradation due to high-energy irradiation as described in chapter 3.4.

3.3.3 Photo-Induced Phase Segregation of Alloyed Perovskites

Alloying ABX_3 perovskites proved to be the route to tailor opto-electronic properties and in particular the band gap. Monovalent cations [$CH_3NH_3^+$, $HC(NH_2)_2^+$, Cs^+, or Rb^+], divalent cations [Pb^{2+} or Sn^{2+}] and halide anions [Br^- or I^-] can be used for A, B and X respectively. Combining halides, for example, allows a continuous tuning of the band-gap energy between 1.5 and 2.2 eV or between 1.8 and 2.4 eV for $MAPb(I_{1-x}Br_x)_3$ [43] and $CsPb(I_{1-x}Br_x)_3$ [159], respectively. This is an important prerequisite for tandem solar cell optimization.

However, the majority of these alloys are not stable under illumination. Photoluminescence measurements reported by Hoke et al. (**figure 8**a), reveal a swift rise of a low-energy emission peak under continuous illumination for $MAPb(I_{1-x}Br_x)_3$ based alloys. [195] A photo-induced phase segregation into iodide rich and bromide rich domains, frequently referred to as the Hoke effect, [196,197] has been suggested. [195] This was corroborated by XRD measurements that revealed the coexistence of both phases after illumination. As a result, photo-induced charge carriers are trapped in the low-energy iodide rich phase. Interestingly, the effect is fully reversible upon thermal annealing in the dark.[195] Figure 8b depicts the temporal evolution of the photo-induced phase segregation on the nanoscale. Bischak et al.[198] overlaid secondary electron (SE) and a cathodoluminescence (CL) images of $MAPb(I_{0.9}Br_{0.1})_3$ before and after illumination. The data show that photo-induced iodine rich clusters grow quickly in size and somewhat slower in number.

The driving force for the photo-induced phase segregation is subject of ongoing research.[195–199] It has been proposed, that the coexistence of both phases corresponds to a local minimum of the Helmholtz free energy. [200] Remarkably, photo-induced phase segregation does not occur when a pulsed excitation is used with a repetition rate of less than 1 kHz. This effect is independent of the excitation energy.[199] This indicates that the phase segregation is governed by a two-step process. [199] To account for the degradation a model has been suggested that postulates the existence of long-lived polaronic states that drive ion migration locally.[198,199] As a result, iodine rich clusters form that have a lower band gap. These clusters are the origin of the low-energy PL emission line. It is interesting to note that segregation of iodine into nanodomains also was observed in highly efficient $(FAPbI_3)_{0.85}(MAPbBr_3)_{0.15}$ solar cells. [201]

As a matter of fact, photo-induced phase segregation is not restricted to $MAPb(I_{1-x}Br_x)_3$ based alloys. It has also been reported for $CsPb(I_{1-x}Br_x)_3$, $FAPb(I_{1-x}Br_x)_3$, $(MA,FA)Pb(I_{1-x}Br_x)_3$, $(Cs_xFA_{1-x})PbI_3$, and $(Cs_{1-y}FA_y)Pb(I_{1-x}Br_x)_3$ alloys. As example figure 8c depicts X-ray diffractograms of $(Cs_{1-x}FA_x)PbI_3$ before and after irradiation. [202] In case of $(Cs_{0.3}FA_{0.7})PbI_3$ a splitting of the XRD reflex of the 110 planes at $2\Theta \approx 14°$ indicates the presence of two coexisting phases after irradiation. Recently, Unger et al. [197] published an overview of the Hoke effect using all available compositional data from literature.[41–43,104,147,159,171,195,199,203–213] As a general trend, substitution of iodine with bromine forms materials with a higher band gap. This is shown in figure 8d where the initial and final PL emission after light soaking is depicted. Above a certain threshold all alloys exhibit a lower energy PL line. The onset is located at ≈1.7 eV and ≈1.9 eV for $MAPb(I_{1-x}Br_x)_3$ and $CsPb(I_{1-x}Br_x)_3$, respectively. In addition, the formation of a lower energy emission line is accompanied by a pinning of the open circuit voltage of perovskite solar cells. This is observed for all alloys with an absorption onset above the aforementioned threshold (see figure 8e). [197]

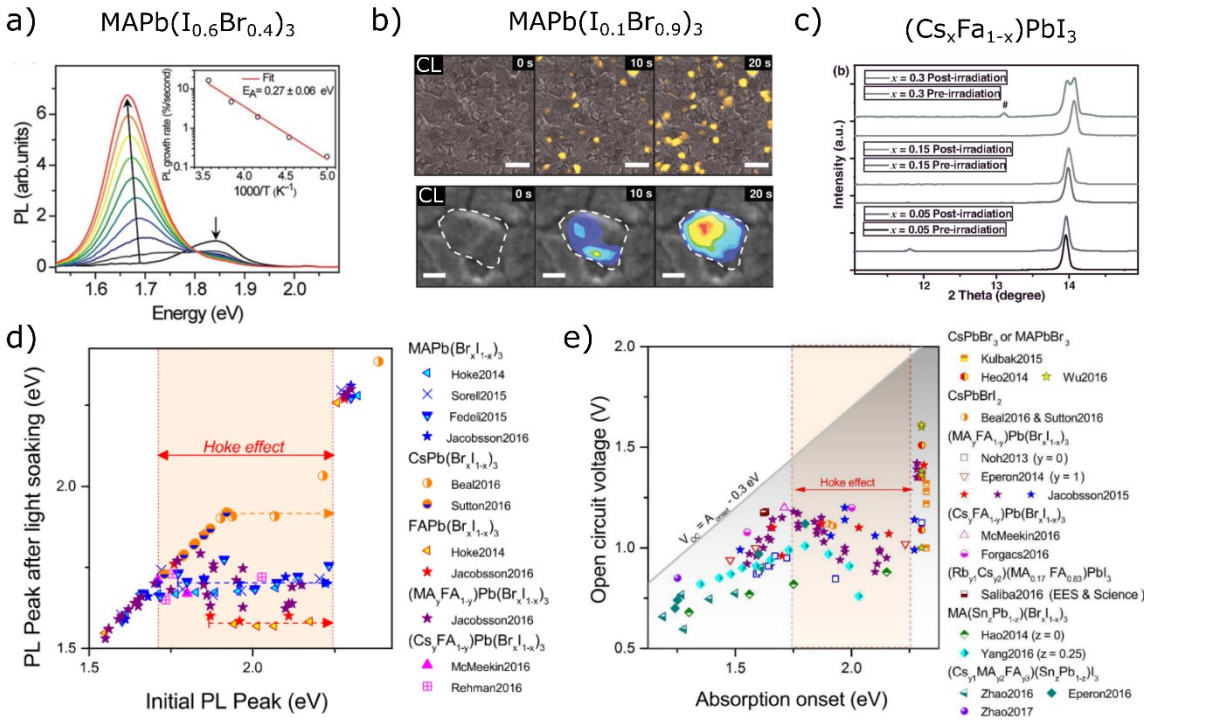

Figure 8. Photo-induced phase segregation of mixed perovskites. (a) Photoluminescence spectra of $MAPb(I_{0.6}Br_{0.4})_3$ under illumination (15 $mWcm^{-2}$, 457 nm, for 45 s). Reproduced with permission. [195] Copyright 2015, The Royal Society of Chemistry. (b) Cathodoluminescence image series after light soaking using a 405 nm LED with a power density of 50 $mWcm^{-2}$. Scale bars are 2 µm (top) and 200 nm (bottom) Reproduced with permission. [198] Copyright 2017, American Chemical Society. (c) X-ray diffractogram of $(Cs_xFA_{1-x})PbI_3$ before and after irradiation. Reproduced with permission. [202] Copyright 2017, John Wiley and Sons.(d) PL emission after light soaking as a function of initial PL peak

energy (e) Open circuit voltage of reported perovskite solar cells as a function of perovskite band gap. (d, e) Reproduced with permission. [197] Copyright 2015, The Royal Society of Chemistry.

The photo-induced phase segregation limits the performance of higher band gap perovskite solar-cells fundamentally. Apparently, a continuous tuning of the band-gap energy is not achievable. However, a band gap of 1.73 eV, which is needed for efficient tandem solar-cells with crystalline Si [47], is achievable using, for example, $CsPb(I_{1-x}Br_x)_3$ or $(Cs_{1-y}FA_y)Pb(I_{1-x}Br_x)_3$ alloys. [147,159,205]

The photo-induced phase segregation is retarded in perovskites that exhibit a long-range crystalline order.[196,205,214] However, the question arises whether light-induced defect generation and/or the presence of heat and moisture etc. will affect the crystalline structure, thereby promoting phase segregation.

3.4. High Energy Irradiation

In addition to the degradation mechanisms discussed above the irradiation with high-energy rays and particles, such as X-rays, γ-rays, electrons, neutrons or protons, can result in detrimental effects on all known inorganic and organic materials. On the other hand, various characterization methods rely on the interaction of a probe beam with the specimen. Any degradation of the specimen during a measurement alters the physical properties of the sample and may produces artifacts that lead to unreliable information and subsequently to a misinterpretation of the data.

Rutherford backscattering spectroscopy, for example, is widely used to obtain depth dependent concentration profiles. [215] Yet the irradiation of a $MAPbI_3$ thin-films with $^4He^+$ ions of an energy of 1.4 MeV causes a swift degradation to PbI_2.[216] Apparently, two or more complementary techniques with orthogonal analysis beam direction have to be used to ensure correct measurements.[216] The chemical structure of hybrid perovskites is commonly determined from X-ray photoelectron spectroscopy (XPS) data. [70,77,88,89,217–229] As example, **figure 9a** depicts XPS spectra of the Pb4f levels of $MAPbI_3$, $MAPbI_{3-x}Cl_x$, $MAPbCl_3$, and $PbCl_2$ thin films. [230] The X-ray energy used for data acquisition amounts to 4 keV. All spectra are dominated by two intense peaks, which can be assigned to the $Pb4f_{5/2}$ and $Pb4f_{7/2}$ levels of Pb^{2+}. At lower binding energies of 137.0 eV and 141.85 eV all perovskite thin-films

exhibit two additional peaks that are reflecting the presence of $Pb^{(0)}$. On the one hand, $Pb^{(0)}$ is often observed in XPS spectra of hybrid perovskites throughout literature. [70,231,232] On the other hand, metallic $Pb^{(0)}$ is not found in spectra of lead halides (figure 9a). Clearly, metallic $Pb^{(0)}$ can be a remnant of an improper preparation and/or annealing procedure. [233] However, it has been shown that the peak attributed to metallic $Pb^{(0)}$ increases in intensity with prolonged X-ray exposure. [230]

Other common tools to study the microstructure and composition of hybrid perovskite films on the nanoscale are electron microscopy and energy dispersive X-ray spectroscopy. Both techniques are widely used but only a few studies paid attention to perovskite degradation during the exposure to low-energy electrons. [234–237] For example, Edri et al. [235] measured electron beam induced current (EBIC) spectra on the cross section of $MAPbI_3$ based solar cells. They observed a strong fading of the EBIC contrast after only 3 consecutive measurements. [235] This low-energy electron-beam-induced degradation of $MAPbI_3$ and $FAPbI_3$ was studied in depth using cathodoluminescence (CL) spectroscopy. [91] Xia et al. [91] showed that an intense electron irradiation energies ranging from 2 to 10 keV can alter the properties of the perovskites. CL spectra measured with an excitation of 5 keV for a variety of electron currents and irradiation times are depicted in figure 9b. The observed changes of the CL spectra are ascribed to two different mechanisms: (i) defect formation caused by radiation damage, and (ii) electron-beam induced heating in case of elevated beam currents. The former mechanism causes quenching and broadening of the excitonic peaks in the CL spectra, whereas the latter one results in the formation of new peaks with higher emission photon energies (see figure 9b).[91]

A further increase of the excitation energy to values in the MeV regime alters the interaction entirely. The penetration depth increases to values in the µm regime and beyond. Nevertheless, electron and proton irradiation in the MeV regime deteriorate inorganic solar cells and electronic devices based on Si, InGaP, GaAs, or Ge vastly. [238–246] Astonishingly, recent findings revealed an unexpectedly high radiation hardness of $MAPbI_3$ based solar cells under high-energetic electron and proton irradiation. [90,92,93] Figure 9c shows *in-situ* measurements of the fill factor, FF, short circuit current, J_{SC}, open circuit voltage, V_{OC}, and power conversion efficiency, η, of a perovskite solar cell as a function of the proton dose, ϕ. The proton had a kinetic energy of 68 MeV. For comparison, the blue line in figure 9c shows J_{SC} of a single crystal silicon (c-Si) diode. Interestingly, for the $MAPbI_3$ based solar cell FF and V_{OC} remain unchanged over the whole course of the proton irradiation. Only J_{SC} decreases to

a values 0.6 for a proton dose of $\phi = 10^{13}$ p cm^{-2}. Note that J_{SC} of the c-Si diode decreases to a value of less than 0.6 for a lower proton dose of $\phi = 10^{12}$ p cm^{-2}. For the perovskite solar cell, it was shown that a major part of the reduction of J_{SC} is due to shading caused by the formation of color centers in the glass substrate. [90] It was concluded that the radiation hardness of $MAPbI_3$ exceeds the radiation hardness of c-Si by almost three orders of magnitude. [90]

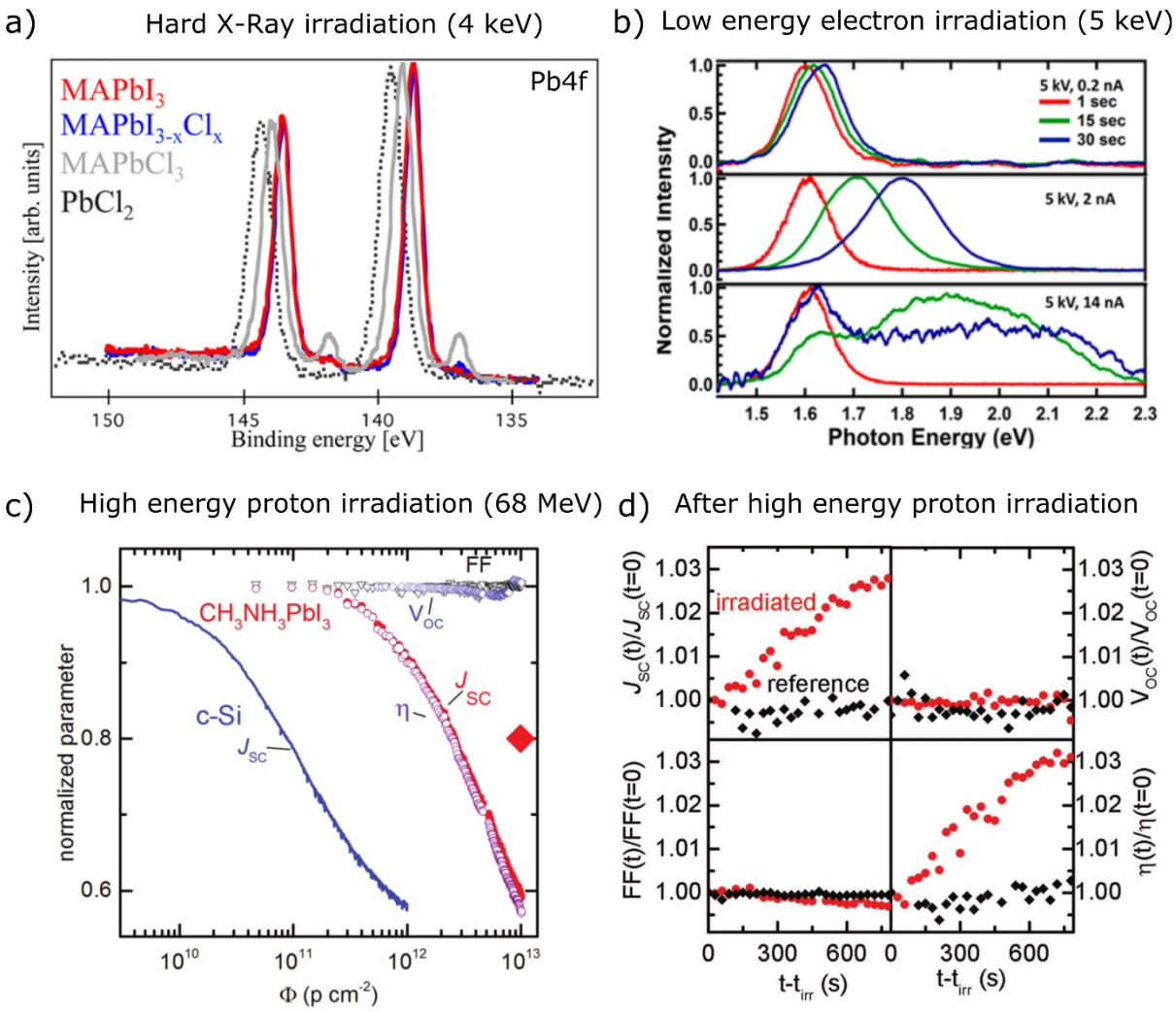

Figure 9. Degradation of hybrid perovskites due to high-energy irradiation. a) Hard X-ray photoelectron spectra of the Pb4f levels of $MAPbI_3$, $MAPbI_{3-x}Cl_x$, $MAPbCl_3$ and $PbCl_2$ thin films on glass/FTO/TiO_2 substrates using a photon energy of 4 keV. Reproduced with permission. [230] Copyright 2015, American Chemical Society. b) Cathodoluminescence spectra of $MAPbI_3$ thin films under excitation with high-energy electrons (E_e = 5 kV). The irradiation times and electron currents are indicated in the figure. Reproduced with permission. [91] Copyright 2015, American Chemical Society. c) Normalized solar cell parameters of a $CH_3NH_3PbI_3$ solar cell under high-energy proton irradiation (E_P = 68 MeV) as a function of the proton dose, ϕ. The red diamond depicts the normalized value of J_{SC} after correcting for shading losses due to the creation of color centers in the substrate. For comparison, the

evolution of a c-Si photo-diode is shown by the blue solid curve. d) Self-healing of a proton-irradiated perovskite solar cell (red circles) after terminating the proton irradiation. Data points are normalized to unity at $t - t_{irr} = 0$. (c, d) Reproduced with permission. [90] Copyright 2016, John Wiley and Sons.

After termination of the proton irradiation the $MAPbI_3$ based solar cells are stored in the dark for 2 weeks to allow the induced radioactivity to decrease. After that time the solar cells show a partial recover of J_{SC} and η (see figure 9d). In fact, it has been shown that the density of recombination centers in the $MAPbI_3$ absorber layer is significantly reduced after these 2 weeks. [93] As a result, V_{OC}, FF, and the recombination lifetime of photo-generated charge carries are higher in proton-irradiated devices compared to non-irradiated reference devices. [90,93]

The question arises if the self-healing is caused by the same mechanism that is responsible for the recovery of perovskite solar cells after prolonged illumination with photons in the UV/Vis energy range (see figure 6a and 6c in chapter 3.3.2). It is known that high-energy electron and proton irradiation generates cascades of secondary electrons with high energies. It is conceivable, that the secondary electrons can cause bond breaking of N-H and C-H bonds of the organic cations prior to thermalization to the conduction band-edge.[90] The dissociation of C-H bonds upon irradiation is well-known in organic semiconductors such as PCDTBT or P3HT. [247,248] The governing microscopic mechanism could be similar to the light-induced dissociation of N-H bonds observed for $MAPbI_3$ and $FAPbI_3$ (see chapter 3.3.2 and figure 7). In fact, fragmentation of $CH_3NH_3^+$ gives rise to localized states in the band gap of $MAPbI_3$ and therefore, might account for the degradation of solar cells due to proton irradiation.[187,188] The subsequent self-healing of the solar cells indicates that some of the newly created defects are passivated or neutralized. This may occur as a back reaction of the defect creation process and/or the neutralization of defects due to the formation of neutral complexes e.g.: the capture of a proton.

The superior radiation hardness of $MAPbI_3$ may lead to practical applications. As an example, it is conceivable to integrate perovskite solar cells in tandem devices with radiation hard CIGS [copper indium gallium di-selenide] devices for space applications. Such tandem solar cells would be lightweight, thin, and flexible and have a high power conversion efficiency. Another example would be radiation hard sensors for the nuclear energy sector, medical imaging, and radiotherapy treatments. Even applications for low-energy electron radiation are

conceivable despite of the reported swift degradation of the perovskite (see figure 9b), since low-energy particles can be shielded with a few millimeters of material.

4. Beyond Organic-Inorganic Perovskites

As discussed above, hybrid perovskites are suffering from different types of degradation mechanisms. On the one hand, the temperature and humidity induced degradation pathways can be easily overcome. The former can be avoided by introducing the more robust formamidinium cation into the perovskite lattice, and the latter by introducing different encapsulation layers. On the other hand, photo-induced dissociation of the organic cation is a major drawback (see section 3.3.2). In fact, any photo-instability may impede commercialization of this promising material.

In general, there are various routes to stabilize hybrid perovskites. For example, one could replace the organic cation with a more stable cation. This is possible using cesium based perovskites, following the general formula $CsBX_3$, were X = I, Br and B = Pb, Sn. Interestingly, all inorganic ABX_3 perovskites were introduced even before the organic/inorganic prototypes were available. Early works by Wells and Haupt report on the synthesis and the properties of Cesium, Potassium, and Rubidium lead halide perovskites.[250,251] Nowadays, Cesium containing perovskites are successfully implemented in solar cells. Moreover, cesium lead trihalides have demonstrated a number of properties similar to those of organic/inorganic perovskites. In these perovskites the band gap can be tuned over a wide range. They have a high tolerance for defects, show a high charge carrier mobility, and a long carrier diffusion length. [211,252] Moreover, the inorganic perovskites can be operated at elevated temperatures and do not exhibit light induced degradation. For example, nanocrystals of $CsPbX_3$ perovskite show an extreme luminescence quantum yield at room temperature combined with a broadly tunable band gap (**Figure 10**a).[253,254] In addition, $CsPbI_3$ QDs exhibit strong quantum confinement and allow to obtain solar cells with a stabilized power conversion efficiency of $\eta \approx 8$ % .[255] Recently, Kulbak et al. demonstrated solar cells with open circuit voltages as high as 1.3 V using bulk $CsPbBr_3$ layers that were sandwiched between FTO/TiO_2 and a hole-transport-layer/Au contacts (figure 10b).[208] Subsequently, several groups reported on efficient cesium based perovskite solar-cells. [211,256,257] Using $CsPbI_3$, the best performing devices had an efficiency of more than 9 %. [211] Unfortunately, none of the previously reported materials of the $APbX_3$ structure form a thermodynamically stable perovskite phase, which is photoactive and typically called “black

phase". The reason for this instability was found in the slightly smaller tolerance factor, due to the mismatch of the ionic radius of the inorganic A-site (Cs, Rb, K) cation within the lead iodide octahedral structure.

Nevertheless, early work on inorganic perovskites by Wells and Haupt revealed that iodoplumbates of Cs, Rb, and potassium form stable materials that adopt a different stoichiometry, namely $A_mB_nX_{2n+m}$, where m = 2 and n = 1. Latest results of computational screening revealed that potential candidates for optoelectronic devices could be found among a broader range of stoichiometric ratio - $A_mB_nX_y$. Moreover, hypothetical $A_mB_nX_y$ perovskites have less restrictions regarding the valences of the metallic cation, namely B = B^{2+} (Sn, Ge), B^{3+} (Bi, Sb), or B^{4+} (Figure 10c).[258,259]

Recently, inorganic alloys Ag_2PbI_4 and $AgBi_2I_7$ were for the first time implemented into devices and yielded an efficiency of η = 3.9 and 1.22 %, respectively (Figure 10 (d)).[260,261] A further alternative approach to obtain stable perovskites is the heterovalent substitution of the B-site cation with B^{1+} and B^{3+}, which allows to obtain "double perovskite" structures.[262–264] The material Cs_2AgBiX_6 shows a moderately long recombination lifetime of $\tau \geq 660$ ns and a band gap of $E_G \sim 1.95$ eV for $Cs_2AgBiBr_6$ and $E_G \sim 2.7$ eV was observed for Cs_2AgBiI_6.[265,266]

Recent computational research to design and identify new potential hybrid perovskites is based mainly on quaternary ammonium compounds.[267,268] However, N − H bonds play a major role in the light-induced degradation mechanism of organic/inorganic perovskites (see chapter 3.3.2). Therefore, we would like to point out that for the design of stable hybrid perovskites organic cations might have to be considered that do not contain weak bonds. Altogether, these interesting and diverse approaches have the potential to overcome the deficiencies described above and lead to new perovskites with a long-time stability and the potential for high efficiency solar cells.

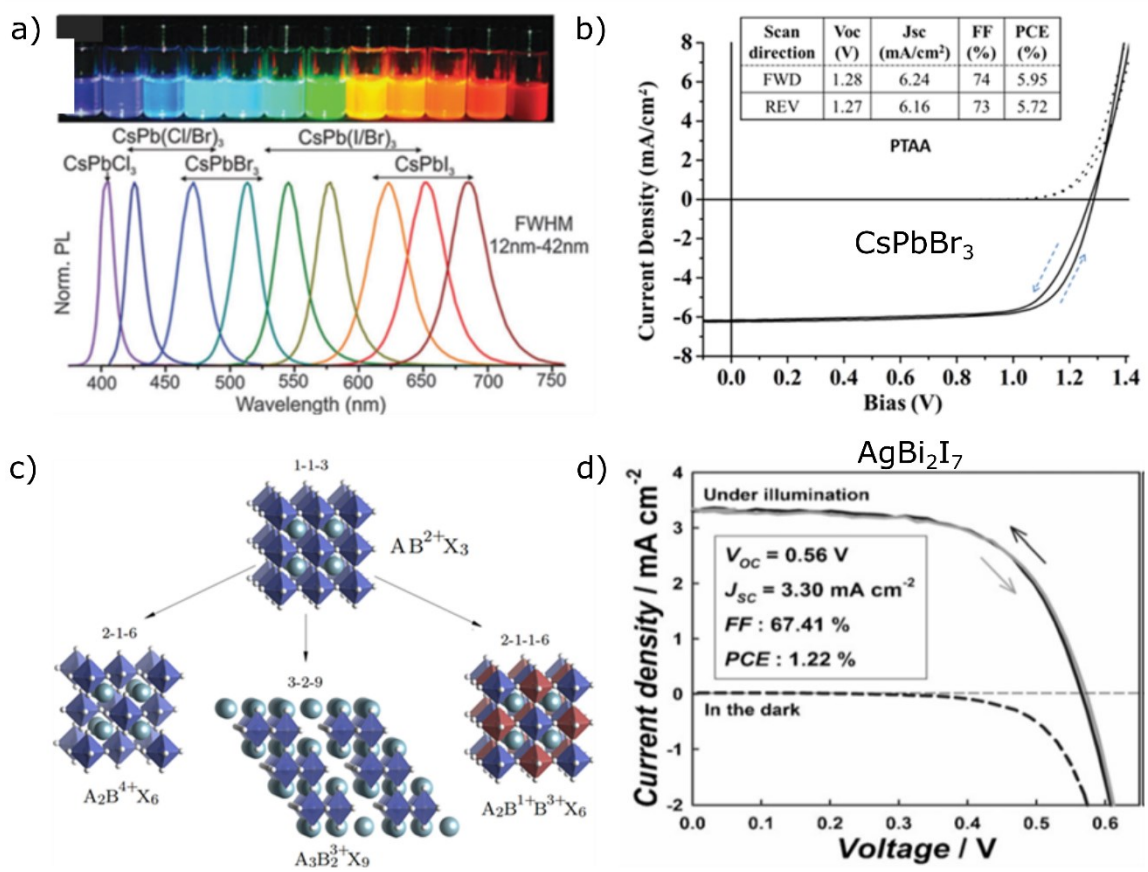

Figure 9. Beyond organic-inorganic perovskites: a) Colloidal perovskite $CsPbX_3$ nanocrystals (X = Cl, Br, I) in toluene under UV excitation and corresponding PL spectra. Reproduced with permission.[254] Copyright 2015, American Chemical Society. b) Light and dark *J–V* curves of mp-TiO_2/$CsPbBr_3$ solar cells with PTAA as a hole transport layer (100 mW/cm^2 simulated solar irradiation, masked cell area 0.16 cm^2, scan rate 0.06 V/s). Reproduced with permission.[208] Copyright 2015, American Chemical Society c) Schematic depiction of the relation between the crystal structures of Pb perovskites and $A_mB_nX_y$ perovskites, where B-site cation has the different oxidation states, and double perovskites. Reproduced with permission.[264] Copyright 2016, American Chemical Society d) *J*-V curves of amp-TiO_2/$AgBi_2I_7$/P3HT/Ag solar cell in the dark and under illumination with a light density of 100 mWcm^2 (area = 0.049 cm2). Reproduced with permission.[261] Copyright 2016, John Wiley and Sons.

5. Conclusion

In conclusion, we thoroughly analyzed T_{80} lifetimes of various perovskite solar cells by comparing over 50 publications reported in literature. Often lifetimes are given for storing devices in the dark and a considerable reduction of the lifetime is reported under illumination

conditions. However, in the past years considerable progress was made regarding the stabilities of solar cells. The known mechanisms that are responsible for the degradation of perovskite solar cells were reviewed and their impact was evaluated. Among the degradation mechanisms are the influence of moisture, heat, photo-induced phase segregation in mixed cation mixed halide perovskites, oxygen catalyzed degradation, photo-induced dissociation of organic cations, and high-energy irradiation. Alternative approaches to overcome materials and device instabilities were suggested. They comprise the use of inorganic perovskites, crystal structures of the type $A_mB_nX_y$, double perovskites, and approaches to eliminate weak bonds in the organic cations.

6. Experimental Section

T_{80} lifetimes were taken from various reports throughout literature. [41–43,46,64,73,81,84,95–141] Note that the lifetimes were extracted manually from plotted stability data. Naturally, this introduces some inaccuracy. However, stability of perovskite solar cells differs vastly from device to device, even under identical fabrication conditions, as published elsewere. [162] As most reports do not average multiple measurements, the inaccuracy of our manual data extraction is of minor importance.

Polycrystalline $FAPbI_3$ thin films were prepared on cleaned silicon substrates. Therefore, 1.1 M of PbI_2 and $HC(NH_2)_2I$ were dissolved in anhydrous dimethylformamide. The precursor solution was subsequently spin coated at 1000 rpm for 10 s, at 2000 rpm for 20 s, and finally at 5000 rpm for 20 s. Subsequent crystallization at 200°C for 20 min yielded an about 2 µm thick $FAPbI_3$ layer. The average grain size was 360 nm. Owing to the poor stability of organo-metal perovskites, spin coating and crystallization was performed in inert atmosphere. FT-IR spectra were recorded after transfer of the specimens in an N_2 filled container. To avoid infrared absorption from air the FT-IR measurements were performed in vacuum.

Acknowledgements
The authors would like to thank E. Unger, S. Albrecht, C. Hartmann and A. Abate for helpful discussions. One of the authors, V.V.B., acknowledges financial support from the Alexander-von-Humboldt Foundation. O. S. is pleased to acknowledge financial support from the graduate school ‘Hybrid4Energy’.

Received: ((will be filled in by the editorial staff))
Revised: ((will be filled in by the editorial staff))
Published online: ((will be filled in by the editorial staff))

References

[1] C. C. Stoumpos, C. D. Malliakas, M. G. Kanatzidis, *Inorg. Chem.* **2013**, *52*, 9019.

[2] G. Xing, N. Mathews, S. S. Lim, N. Yantara, X. Liu, D. Sabba, M. Grätzel, S. Mhaisalkar, T. C. Sum, *Nat. Mater.* **2014**, *13*, 476.

[3] S. D. Stranks, G. E. Eperon, G. Grancini, C. Menelaou, M. J. P. Alcocer, T. Leijtens, L. M. Herz, A. Petrozza, H. J. Snaith, *Science* **2013**, *342*, 341.

[4] T. Dittrich, F. Lang, O. Shargaieva, J. Rappich, N. H. Nickel, E. Unger, B. Rech, *Appl. Phys. Lett.* **2016**, *109*, 73901.

[5] Y.-H. Kim, H. Cho, J. H. Heo, T.-S. Kim, N. Myoung, C.-L. Lee, S. H. Im, T.-W. Lee, *Adv. Mater.* **2015**, *27*, 1248.

[6] S. A. Veldhuis, P. P. Boix, N. Yantara, M. Li, T. C. Sum, N. Mathews, S. G. Mhaisalkar, *Adv. Mater.* **2016**, *28*, 6804.

[7] Z.-K. Tan, R. S. Moghaddam, M. L. Lai, P. Docampo, R. Higler, F. Deschler, M. Price, A. Sadhanala, L. M. Pazos, D. Credgington, F. Hanusch, T. Bein, H. J. Snaith, R. H. Friend, *Nat. Nanotechnol.* **2014**, *9*, 687.

[8] O. A. Jaramillo-Quintero, R. S. Sanchez, M. Rincon, I. Mora-Sero, *J. Phys. Chem. Lett.* **2015**, *6*, 1883.

[9] D. Liang, Y. Peng, Y. Fu, M. J. Shearer, J. Zhang, J. Zhai, Y. Zhang, R. J. Hamers, T. L. Andrew, S. Jin, *ACS Nano* **2016**, *10*, 6897.

[10] J. Li, S. G. R. Bade, X. Shan, Z. Yu, *Adv. Mater.* **2015**, *27*, 5196.

[11] J. Pan, L. N. Quan, Y. Zhao, W. Peng, B. Murali, S. P. Sarmah, M. Yuan, L. Sinatra, N. M. Alyami, J. Liu, E. Yassitepe, Z. Yang, O. Voznyy, R. Comin, M. N. Hedhili, O. F. Mohammed, Z. H. Lu, D. H. Kim, E. H. Sargent, O. M. Bakr, *Adv. Mater.* **2016**, *28*, 8718.

[12] Z. Chen, C. Zhang, X.-F. Jiang, M. Liu, R. Xia, T. Shi, D. Chen, Q. Xue, Y.-J. Zhao, S.

Su, H.-L. Yip, Y. Cao, *Adv. Mater.* **2017**, *29*, 1603157.

[13] X. Y. Chin, D. Cortecchia, J. Yin, A. Bruno, C. Soci, *Nat. Commun.* **2015**, *6*, 1.

[14] X. Liu, L. Niu, C. Wu, C. Cong, H. Wang, Q. Zeng, H. He, Q. Fu, W. Fu, T. Yu, C. Jin, Z. Liu, T. C. Sum, *Adv. Sci.* **2016**, *3*, 1600137.

[15] T. S. Kao, Y.-H. Chou, C.-H. Chou, F.-C. Chen, T.-C. Lu, *Appl. Phys. Lett.* **2014**, *105*, 231108.

[16] R. Dhanker, A. N. Brigeman, A. V. Larsen, R. J. Stewart, J. B. Asbury, N. C. Giebink, *Appl. Phys. Lett.* **2014**, *105*, 151112.

[17] Y. Fu, H. Zhu, A. W. Schrader, D. Liang, Q. Ding, P. Joshi, L. Hwang, X.-Y. Y. Zhu, S. Jin, *Nano Lett.* **2016**, *16*, 1000.

[18] S. Yakunin, L. Protesescu, F. Krieg, M. I. Bodnarchuk, G. Nedelcu, M. Humer, G. De Luca, M. Fiebig, W. Heiss, M. V. Kovalenko, *Nat. Commun.* **2015**, *6*, 8056.

[19] F. Deschler, M. Price, S. Pathak, L. E. Klintberg, D.-D. Jarausch, R. Higler, S. Hüttner, T. Leijtens, S. D. Stranks, H. J. Snaith, M. Atatüre, R. T. Phillips, R. H. Friend, *J. Phys. Chem. Lett.* **2014**, *5*, 1421.

[20] B. R. Sutherland, S. Hoogland, M. M. Adachi, C. T. O. Wong, E. H. Sargent, *ACS Nano* **2014**, *8*, 10947.

[21] S. Chen, K. Roh, J. Lee, W. K. Chong, Y. Lu, N. Mathews, T. C. Sum, A. Nurmikko, *ACS Nano* **2016**, *10*, 3959.

[22] Y. Fu, H. Zhu, C. C. Stoumpos, Q. Ding, J. Wang, M. G. Kanatzidis, X. Zhu, S. Jin, *ACS Nano* **2016**, *10*, 7963.

[23] M. Saliba, S. M. Wood, J. B. Patel, P. K. Nayak, J. Huang, J. A. Alexander-Webber, B. Wenger, S. D. Stranks, M. T. Hörantner, J. T.-W. Wang, R. J. Nicholas, L. M. Herz, M. B. Johnston, S. M. Morris, H. J. Snaith, M. K. Riede, *Adv. Mater.* **2016**, *28*, 923.

[24] K. C. Kwon, K. Hong, Q. Van Le, S. Y. Lee, J. Choi, K.-B. Kim, S. Y. Kim, H. W. Jang, *Adv. Funct. Mater.* **2016**, *26*, 4213.

[25] K. Domanski, W. Tress, T. Moehl, M. Saliba, M. K. Nazeeruddin, M. Grätzel, *Adv. Funct. Mater.* **2015**, *25*, 6936.

[26] Y. Lee, J. Kwon, E. Hwang, C.-H. Ra, W. J. Yoo, J.-H. Ahn, J. H. Park, J. H. Cho, *Adv. Mater.* **2015**, *27*, 41.

[27] B. R. Sutherland, A. K. Johnston, A. H. Ip, J. Xu, V. Adinolfi, P. Kanjanaboos, E. H. Sargent, *ACS Photonics* **2015**, *2*, 1117.

[28] Y. Fang, Q. Dong, Y. Shao, Y. Yuan, J. Huang, *Nat. Photonics* **2015**, *9*, 679.

[29] C. Liu, K. Wang, P. Du, E. Wang, X. Gong, A. J. Heeger, *Nanoscale* **2015**, *7*, 16460.

[30] Z. Lian, Q. Yan, Q. Lv, Y. Wang, L. Liu, L. Zhang, S. Pan, Q. Li, L. Wang, J.-L. L. Sun, *Sci. Rep.* **2015**, *5*, 16563.

[31] R. Dong, Y. Fang, J. Chae, J. Dai, Z. Xiao, Q. Dong, *Adv. Mater.* **2015**, 1.

[32] M. He, Y. Chen, H. Liu, J. Wang, X. Fang, Z. Liang, *Chem. Commun.* **2015**, 3.

[33] V. Adinolfi, O. Ouellette, M. I. Saidaminov, G. Walters, A. L. Abdelhady, O. M. Bakr, E. H. Sargent, *Adv. Mater.* **2016**, *28*, 7264.

[34] S. Chen, C. Teng, M. Zhang, Y. Li, D. Xie, G. Shi, *Adv. Mater.* **2016**, *28*, 5969.

[35] Y. Wang, Z. Xia, S. Du, F. Yuan, Z. Li, Z. Li, Q. Dai, H. Wang, S. Luo, S. Zhang, H. Zhou, *Nanotechnology* **2016**, *27*, 175201.

[36] F. Wang, J. Mei, Y. Wang, L. Zhang, H. Zhao, D. Zhao, *ACS Appl. Mater. Interfaces* **2016**, *8*, 2840.

[37] C. Liu, K. Wang, P. Du, E. Wang, X. Gong, A. J. Heeger, *Nanoscale* **2015**, *7*, 16460.

[38] M. He, Y. Chen, H. Liu, J. Wang, X. Fang, Z. Liang, *Chem. Commun.* **2015**, 3.

[39] H. Rao, W. Li, B. Chen, D. Kuang, C. Su, *Adv. Mater.* **2017**, *29*, 1602639.

[40] Y. Lee, J. Kwon, E. Hwang, C.-H. Ra, W. J. Yoo, J.-H. Ahn, J. H. Park, J. H. Cho, *Adv. Mater.* **2015**, *27*, 41.

[41] M. Saliba, T. Matsui, K. Domanski, J.-Y. Seo, A. Ummadisingu, S. M. Zakeeruddin, J.-P. Correa-Baena, W. R. Tress, A. Abate, A. Hagfeldt, M. Grätzel, *Science* **2016**, *354*,

206.

[42] M. Saliba, T. Matsui, J.-Y. Seo, K. Domanski, J.-P. Correa-Baena, M. K. Nazeeruddin, S. M. Zakeeruddin, W. Tress, A. Abate, A. Hagfeldt, M. Grätzel, *Energy Environ. Sci.* **2016**, *9*, 1989.

[43] J. H. Noh, S. H. Im, J. H. Heo, T. N. Mandal, S. Il Seok, *Nano Lett.* **2013**, *13*, 1764.

[44] S. Albrecht, M. Saliba, J. P. Correa Baena, F. Lang, L. Kegelmann, M. Mews, L. Steier, A. Abate, J. Rappich, L. Korte, R. Schlatmann, M. K. Nazeeruddin, A. Hagfeldt, M. Grätzel, B. Rech, *Energy Environ. Sci.* **2016**, *9*, 81.

[45] F. Lang, M. A. Gluba, S. Albrecht, J. Rappich, L. Korte, B. Rech, N. H. Nickel, *J. Phys. Chem. Lett.* **2015**, *6*, 2745.

[46] K. A. Bush, A. F. Palmstrom, Z. J. Yu, M. Boccard, R. Cheacharoen, J. P. Mailoa, D. P. McMeekin, R. L. Z. Hoye, C. D. Bailie, T. Leijtens, I. M. Peters, M. C. Minichetti, N. Rolston, R. Prasanna, S. Sofia, D. Harwood, W. Ma, F. Moghadam, H. J. Snaith, T. Buonassisi, Z. C. Holman, S. F. Bent, M. D. McGehee, *Nat. Energy* **2017**, *2*, 17009.

[47] S. Albrecht, M. Saliba, J.-P. Correa-Baena, K. Jäger, L. Korte, A. Hagfeldt, M. Grätzel, B. Rech, *J. Opt.* **2016**, *18*, 64012.

[48] R. G. Wilks, M. Bär, *Nat. Energy* **2017**, *2*, 16204.

[49] S. Yang, W. Fu, Z. Zhang, H. Chen, C.-Z. Li, *J. Mater. Chem. A* **2017**, DOI 10.1039/C7TA00366H.

[50] A. H. Slavney, R. W. Smaha, I. C. Smith, A. Jaffe, D. Umeyama, H. I. Karunadasa, *Inorg. Chem.* **2017**, *56*, 46.

[51] X. Zhao, N.-G. Park, *Photonics* **2015**, *2*, 1139.

[52] J. Schoonman, *Chem. Phys. Lett.* **2015**, *619*, 193.

[53] J. Yang, T. L. Kelly, *Inorg. Chem.* **2017**, *56*, 92.

[54] N. Aristidou, I. Sanchez-Molina, T. Chotchuangchutchaval, M. Brown, L. Martinez, T. Rath, S. A. Haque, *Angew. Chemie Int. Ed.* **2015**, *54*, 8208.

[55] W.-J. Yin, T. Shi, Y. Yan, *Appl. Phys. Lett.* **2014**, *104*, 63903.

[56] A. Merdasa, M. Bag, Y. Tian, E. Källman, A. Dobrovolsky, I. G. Scheblykin, *J. Phys. Chem. C* **2016**, *120*, 10711.

[57] W. Nie, J. C. Blancon, A. J. Neukirch, K. Appavoo, H. Tsai, M. Chhowalla, M. A. Alam, M. Y. Sfeir, C. Katan, J. Even, S. Tretiak, J. J. Crochet, G. Gupta, A. D. Mohite, *Nat Commun* **2016**, *7*, 11574.

[58] D. Bryant, N. Aristidou, S. Pont, I. Sanchez-Molina, T. Chotchunangatchaval, S. Wheeler, J. R. Durrant, S. A. Haque, *Energy Environ. Sci.* **2016**, *9*, 1655.

[59] G. Murugadoss, S. Tanaka, G. Mizuta, S. Kanaya, H. Nishino, T. Umeyama, H. Imahori, S. Ito, *Jpn. J. Appl. Phys.* **2015**, *54*, 08KF08.

[60] A. Dualeh, P. Gao, S. Il Seok, M. K. Nazeeruddin, M. Grätzel, *Chem. Mater.* **2014**, *26*, 6160.

[61] R. K. Misra, S. Aharon, B. Li, D. Mogilyansky, I. Visoly-Fisher, L. Etgar, E. A. Katz, *J. Phys. Chem. Lett.* **2015**, *6*, 326.

[62] B. Conings, J. Drijkoningen, N. Gauquelin, A. Babayigit, J. D'Haen, L. D'Olieslaeger, A. Ethirajan, J. Verbeeck, J. Manca, E. Mosconi, F. De Angelis, H.-G. Boyen, *Adv. Energy Mater.* **2015**, *5*, 1500477.

[63] D. P. Nenon, J. A. Christians, L. M. Wheeler, J. L. Blackburn, E. M. Sanehira, B. Dou, M. L. Olsen, K. Zhu, J. J. Berry, J. M. Luther, *Energy Environ. Sci.* **2016**, *9*, 2072.

[64] Y.-B. Cheng, Y. Han, S. Meyer, Y. Dkhissi, K. Weber, J. M. J. Pringle, U. Bach, L. Spiccia, Y.-B. Cheng, *J. Mater. Chem. A* **2015**, *3*, 8139.

[65] Z. Song, S. C. Watthage, A. B. Phillips, B. L. Tompkins, R. J. Ellingson, M. J. Heben, *Chem. Mater.* **2015**, *27*, 4612.

[66] T. Supasai, N. Rujisamphan, K. Ullrich, A. Chemseddine, T. Dittrich, *Appl. Phys. Lett.* **2013**, *103*, 183906.

[67] Y. Yuan, J. Chae, Y. Shao, Q. Wang, Z. Xiao, A. Centrone, J. Huang, *Adv. Energy*

Mater. **2015**, *5*, 1500615.

[68] Q. Jeangros, M. Duchamp, J. Werner, M. Kruth, R. E. Dunin-Borkowski, B. Niesen, C. Ballif, A. Hessler-Wyser, *Nano Lett.* **2016**, *16*, 7013.

[69] Y. Yuan, Q. Wang, Y. Shao, H. Lu, T. Li, A. Gruverman, J. Huang, *Adv. Energy Mater.* **2016**, *6*, 1.

[70] W. Huang, J. S. Manser, P. V. Kamat, S. Ptasinska, *Chem. Mater.* **2016**, *28*, 303.

[71] X. Dong, X. Fang, M. Lv, B. Lin, S. Zhang, J. Ding, N. Yuan, *J. Mater. Chem. A* **2015**, *3*, 5360.

[72] X. Gong, M. Li, X.-B. Shi, H. Ma, Z.-K. Wang, L.-S. Liao, *Adv. Funct. Mater.* **2015**, *25*, 6671.

[73] W. Xiang, Q. Chen, Y. Wang, M. Liu, F. Huang, T. Bu, T. Wang, Y.-B. Cheng, X. Gong, J. Zhong, P. Liu, X. Yao, X. Zhao, *J. Mater. Chem. A* **2017**, *5*, 5486.

[74] E. Mosconi, J. M. Azpiroz, F. De Angelis, *Chem. Mater.* **2015**, *27*, 4885.

[75] L. Zhang, P. H.-L. Sit, *J. Phys. Chem. C* **2015**, *119*, 22370.

[76] C. Müller, T. Glaser, M. Plogmeyer, M. Sendner, S. Döring, A. A. Bakulin, C. Brzuska, R. Scheer, M. S. Pshenichnikov, W. Kowalsky, A. Pucci, R. Lovrinčić, *Chem. Mater.* **2015**, *27*, 7835.

[77] Y. Li, X. Xu, C. Wang, C. Wang, F. Xie, J. Yang, Y. Gao, *J. Phys. Chem. C* **2015**, *119*, 23996.

[78] Z. Song, A. Abate, S. C. Watthage, G. K. Liyanage, A. B. Phillips, U. Steiner, M. Graetzel, M. J. Heben, *Adv. Energy Mater.* **2016**, *6*, 1600846.

[79] W. Zhou, Y. Zhao, C. Shi, H. Huang, J. Wei, R. Fu, K. Liu, D. Yu, Q. Zhao, *J. Phys. Chem. C* **2016**, *120*, 4759.

[80] C. Qin, T. Matsushima, T. Fujihara, W. J. Potscavage, C. Adachi, *Adv. Mater.* **2016**, *28*, 466.

[81] J.-W. Lee, D.-H. Kim, H.-S. Kim, S.-W. Seo, S. M. Cho, N.-G. Park, *Adv. Energy*

Mater. **2015**, *5*, 1501310.

[82] G. E. Eperon, S. N. Habisreutinger, T. Leijtens, B. J. Bruijnaers, J. J. van Franeker, D. W. DeQuilettes, S. Pathak, R. J. Sutton, G. Grancini, D. S. Ginger, R. A. J. Janssen, A. Petrozza, H. J. Snaith, *ACS Nano* **2015**, *9*, 9380.

[83] C.-J. Tong, W. Geng, Z.-K. Tang, C.-Y. Yam, X. Fan, J. Liu, W.-M. Lau, L.-M. Liu, *J. Phys. Chem. Lett.* **2015**, *6*, 3289.

[84] I. Hwang, I. Jeong, J. Lee, M. J. Ko, K. Yong, *ACS Appl. Mater. Interfaces* **2015**, *7*, 17330.

[85] Q. Jiang, D. Rebollar, J. Gong, E. L. Piacentino, C. Zheng, T. Xu, *Angew. Chemie Int. Ed.* **2015**, *54*, 7617.

[86] J. Yang, B. D. Siempelkamp, D. Liu, T. L. Kelly, *ACS Nano* **2015**, *9*, 1955.

[87] K. K. Bass, R. E. McAnally, S. Zhou, P. I. Djurovich, M. E. Thompson, B. C. Melot, *Chem. Commun.* **2014**, *50*, 15819.

[88] A. Alberti, I. Deretzis, G. Pellegrino, C. Bongiorno, E. Smecca, G. Mannino, F. Giannazzo, G. G. Condorelli, N. Sakai, T. Miyasaka, C. Spinella, A. La Magna, *ChemPhysChem* **2015**, *16*, 3064.

[89] Y. Li, X. Xu, C. Wang, C. Wang, F. Xie, J. Yang, Y. Gao, *J. Phys. Chem. C* **2015**, *119*, 23996.

[90] F. Lang, N. H. Nickel, J. Bundesmann, S. Seidel, A. Denker, S. Albrecht, V. V. Brus, J. Rappich, B. Rech, G. Landi, H. C. Neitzert, *Adv. Mater.* **2016**, *28*, 8726.

[91] C. Xiao, Z. Li, H. Guthrey, J. Moseley, Y. Yang, S. Wozny, H. Moutinho, B. To, J. J. Berry, B. Gorman, Y. Yan, K. Zhu, M. Al-Jassim, *J. Phys. Chem. C* **2015**, *119*, 26904.

[92] Y. Miyazawa, M. Ikegami, T. Miyasaka, T. Ohshima, M. Imaizumi, K. Hirose, in *2015 IEEE 42nd Photovolt. Spec. Conf.*, IEEE, **2015**, pp. 1–4.

[93] V. V Brus, F. Lang, J. Bundesmann, S. Seidel, A. Denker, B. Rech, G. Landi, H. C. Neitzert, J. Rappich, N. H. Nickel, *Adv. Electron. Mater.* **2017**, *3*, 1600438.

[94] T. A. Berhe, W.-N. Su, C.-H. Chen, C.-J. Pan, J.-H. Cheng, H.-M. Chen, M.-C. Tsai, L.-Y. Chen, A. A. Dubale, B.-J. Hwang, *Energy Environ. Sci.* **2016**, *9*, 323.

[95] J.-H. Im, C.-R. Lee, J.-W. Lee, S.-W. Park, N.-G. Park, *Nanoscale* **2011**, *3*, 4088.

[96] H.-S. Kim, C.-R. Lee, J.-H. Im, K.-B. Lee, T. Moehl, A. Marchioro, S.-J. Moon, R. Humphry-Baker, J.-H. Yum, J. E. Moser, M. Grätzel, N.-G. Park, *Sci. Rep.* **2012**, *2*, 591.

[97] Y. S. Kwon, J. Lim, H.-J. Yun, Y.-H. Kim, T. Park, *Energy Environ. Sci.* **2014**, *7*, 1454.

[98] L. Chen, X. Xie, Z. Liu, E.-C. Lee, *J. Mater. Chem. A* **2017**, *5*, 6974.

[99] W. Yan, Y. Li, Y. Li, S. Ye, Z. Liu, S. Wang, Z. Bian, C. Huang, *Nano Res.* **2015**, *8*, 2474.

[100] J. Ye, X. Zhang, L. Zhu, H. Zheng, G. Liu, H. Wang, T. Hayat, X. Pan, S. Dai, *Sustain. Energy Fuels* **2017**, DOI 10.1039/C7SE00036G.

[101] J. H. Heo, M. H. Lee, H. J. Han, B. R. Patil, J. S. Yu, S. H. Im, *J. Mater. Chem. A* **2016**, *4*, 1572.

[102] J. H. Heo, S. H. Im, D. H. Song, H. J. Han, S. Y. Kim, J. H. Kim, D. Kim, H. W. Shin, T. K. Ahn, C. Wolf, T.-W. Lee, S. H. Im, *Adv. Mater.* **2015**, *27*, 3424.

[103] L. Zheng, Y.-H. Chung, Y. Ma, L. Zhang, L. Xiao, Z. Chen, S. Wang, B. Qu, Q. Gong, *Chem. Commun.* **2014**, *50*, 11196.

[104] J. Zhao, K. O. Brinkmann, T. Hu, N. Pourdavoud, T. Becker, T. Gahlmann, R. Heiderhoff, A. Polywka, P. Görrn, Y. Chen, B. Cheng, T. Riedl, *Adv. Energy Mater.* **2017**, 1602599.

[105] H. Choi, C.-K. Mai, H.-B. Kim, J. Jeong, S. Song, G. C. Bazan, J. Y. Kim, A. J. Heeger, *Nat. Commun.* **2015**, *6*, 7348.

[106] Q. Tai, P. You, H. Sang, Z. Liu, C. Hu, H. L. W. Chan, F. Yan, *Nat. Commun.* **2016**, *7*, 11105.

[107] S. N. Habisreutinger, T. Leijtens, G. E. Eperon, S. D. Stranks, R. J. Nicholas, H. J.

Snaith, *Nano Lett.* **2014**, *14*, 5561.

[108] W. Chen, Y. Wu, Y. Yue, J. Liu, W. Zhang, X. Yang, H. Chen, E. Bi, I. Ashraful, M. Grätzel, L. Han, *Science* **2015**, *350*, 944.

[109] M. Zhang, M. Lyu, H. Yu, J.-H. Yun, Q. Wang, L. Wang, *Chem. - A Eur. J.* **2015**, *21*, 434.

[110] Y. Hou, H. Zhang, W. Chen, S. Chen, C. O. R. Quiroz, H. Azimi, A. Osvet, G. J. Matt, E. Zeira, J. Seuring, N. Kausch-Busies, W. Lövenich, C. J. Brabec, *Adv. Energy Mater.* **2015**, *5*, 1500543.

[111] H. Back, G. Kim, J. Kim, J. Kong, T. K. Kim, H. Kang, H. Kim, J. Lee, S. Lee, K. Lee, *Energy Environ. Sci.* **2016**, *9*, 1258.

[112] G.-W. Kim, G. Kang, J. Kim, G.-Y. Lee, H. Il Kim, L. Pyeon, J. Lee, T. Park, *Energy Environ. Sci.* **2016**, *9*, 2326.

[113] J. A. Christians, P. A. Miranda Herrera, P. V. Kamat, *J. Am. Chem. Soc.* **2015**, *137*, 1530.

[114] Q. Luo, Y. Zhang, C. Liu, J. Li, N. Wang, H. Lin, *J. Mater. Chem. A* **2015**, *3*, 1.

[115] C.-Y. Y. Chang, K.-T. T. Lee, W.-K. K. Huang, H.-Y. Y. Siao, Y.-C. C. Chang, *Chem. Mater.* **2015**, *27*, 5122.

[116] C.-G. Wu, C.-H. Chiang, Z.-L. Tseng, M. K. Nazeeruddin, A. Hagfeldt, M. Grätzel, *Energy Environ. Sci.* **2015**, *8*, 2725.

[117] X. Zhao, H. Shen, Y. Zhang, X. Li, X. Zhao, M. Tai, J. Li, J. Li, X. Li, H. Lin, *ACS Appl. Mater. Interfaces* **2016**, *8*, 7826.

[118] M. R. Leyden, M. V. Lee, S. R. Raga, Y. Qi, *J. Mater. Chem. A* **2015**, *3*, 16097.

[119] N. Lin, J. Qiao, H. Dong, F. Ma, L. Wang, *J. Mater. Chem. A* **2015**, *3*, 22839.

[120] C.-Y. Chang, Y.-C. Chang, W.-K. Huang, K.-T. Lee, A.-C. Cho, C.-C. Hsu, *Chem. Mater.* **2015**, *27*, 7119.

[121] J. Cao, Y.-M. M. Liu, X. Jing, J. Yin, J. Li, B. Xu, Y.-Z. Z. Tan, N. Zheng, *J. Am.*

Chem. Soc. **2015**, *137*, 10914.

[122] A. Mei, X. Li, L. Liu, Z. Ku, T. Liu, Y. Rong, M. Xu, M. Hu, J. Chen, Y. Yang, M. Gratzel, H. Han, *Science* **2014**, *345*, 295.

[123] J. Zhao, X. Zheng, Y. Deng, T. Li, Y. Shao, A. Gruverman, J. Shield, J. Huang, *Energy Environ. Sci.* **2016**, *9*, 3650.

[124] Q. Wang, C. C. Chueh, M. Eslamian, A. K. Y. Jen, *ACS Appl. Mater. Interfaces* **2016**, *8*, 32068.

[125] J. Ye, H. Zheng, L. Zhu, X. Zhang, L. Jiang, W. Chen, G. Liu, X. Pan, S. Dai, *Sol. Energy Mater. Sol. Cells* **2017**, *160*, 60.

[126] W. Ke, D. Zhao, C. R. Grice, A. J. Cimaroli, G. Fang, Y. Yan, *J. Mater. Chem. A* **2015**, *3*, 23888.

[127] L. K. Ono, S. R. Raga, M. Remeika, A. J. Winchester, A. Gabe, Y. Qi, *J. Mater. Chem. A* **2015**, *3*, 15451.

[128] J. P. Correa Baena, L. Steier, W. Tress, M. Saliba, S. Neutzner, T. Matsui, F. Giordano, T. J. Jacobsson, A. R. Srimath Kandada, S. M. Zakeeruddin, A. Petrozza, A. Abate, M. K. Nazeeruddin, M. Grätzel, A. Hagfeldt, *Energy Environ. Sci.* **2015**, *8*, 2928.

[129] Z. Zhu, Y. Bai, X. Liu, C.-C. Chueh, S. Yang, A. K.-Y. Jen, *Adv. Mater.* **2016**, *28*, 6478.

[130] Z. Yu, B. Chen, P. Liu, C. Wang, C. Bu, N. Cheng, S. Bai, Y. Yan, X. Zhao, *Adv. Funct. Mater.* **2016**, *26*, 4866.

[131] M. Kaltenbrunner, G. Adam, E. D. Głowacki, M. Drack, R. Schwödiauer, L. Leonat, D. H. Apaydin, H. Groiss, M. C. Scharber, M. S. White, N. S. Sariciftci, S. Bauer, *Nat. Mater.* **2015**, *14*, 1032.

[132] X. Bao, Y. Wang, Q. Zhu, N. Wang, D. Zhu, J. Wang, A. Yang, R. Yang, *J. Power Sources* **2015**, *297*, 53.

[133] J. H. Heo, H. J. Han, D. Kim, T. K. Ahn, S. H. Im, *Energy Environ. Sci.* **2015**, *8*, 1602.

[134] J. Song, E. Zheng, J. Bian, X.-F. Wang, W. Tian, Y. Sanehira, T. Miyasaka, *J. Mater. Chem. A* **2015**, *3*, 10837.

[135] S. Guarnera, A. Abate, W. Zhang, J. M. Foster, G. Richardson, A. Petrozza, H. J. Snaith, *J. Phys. Chem. Lett.* **2015**, *6*, 432.

[136] F. K. Aldibaja, L. Badia, E. Mas-Marzá, R. S. Sánchez, E. M. Barea, I. Mora-Sero, *J. Mater. Chem. A* **2015**, *3*, 9194.

[137] J. H. Kim, P.-W. Liang, S. T. Williams, N. Cho, C.-C. Chueh, M. S. Glaz, D. S. Ginger, A. K.-Y. Jen, *Adv. Mater.* **2015**, *27*, 695.

[138] Y.-Y. Yu, R.-S. Chiang, H.-L. Hsu, C.-C. Yang, C.-P. Chen, *Nanoscale* **2014**, *6*, 11403.

[139] T. Leijtens, G. E. Eperon, S. Pathak, A. Abate, M. M. Lee, H. J. Snaith, *Nat. Commun.* **2013**, *4*, 2885.

[140] Z. Ku, Y. Rong, M. Xu, T. Liu, H. Han, *Sci. Rep.* **2013**, *3*, 3132.

[141] J. Burschka, N. Pellet, S.-J. Moon, R. Humphry-Baker, P. Gao, M. K. Nazeeruddin, M. Grätzel, *Nature* **2013**, *499*, 316.

[142] M. O. Reese, S. A. Gevorgyan, M. Jørgensen, E. Bundgaard, S. R. Kurtz, D. S. Ginley, D. C. Olson, M. T. Lloyd, P. Morvillo, E. A. Katz, A. Elschner, O. Haillant, T. R. Currier, V. Shrotriya, M. Hermenau, M. Riede, K. R. Kirov, G. Trimmel, T. Rath, O. Inganäs, F. Zhang, M. Andersson, K. Tvingstedt, M. Lira-Cantu, D. Laird, C. McGuiness, S. (Jimmy) Gowrisanker, M. Pannone, M. Xiao, J. Hauch, R. Steim, D. M. DeLongchamp, R. Rösch, H. Hoppe, N. Espinosa, A. Urbina, G. Yaman-Uzunoglu, J.-B. Bonekamp, A. J. J. M. van Breemen, C. Girotto, E. Voroshazi, F. C. Krebs, *Sol. Energy Mater. Sol. Cells* **2011**, *95*, 1253.

[143] NREL, "Research Cell Efficiency Records," can be found under http://www.nrel.gov/ncpv/images/efficiency_chart.jpg, **2016**.

[144] F. Bella, G. Griffini, J.-P. Correa-Baena, G. Saracco, M. Grätzel, A. Hagfeldt, S. Turri, C. Gerbaldi, *Science* **2016**, *354*, 203.

[145] T. Malinauskas, D. Tomkute-Luksiene, R. Sens, M. Daskeviciene, R. Send, H. Wonneberger, V. Jankauskas, I. Bruder, V. Getautis, *ACS Appl. Mater. Interfaces* **2015**, *7*, 11107.

[146] C. Yi, J. Luo, S. Meloni, A. Boziki, N. Ashari-Astani, C. Grätzel, S. M. Zakeeruddin, U. Röthlisberger, M. Grätzel, *Energy Environ. Sci.* **2016**, *9*, 656.

[147] D. P. McMeekin, G. Sadoughi, W. Rehman, G. E. Eperon, M. Saliba, M. T. Horantner, A. Haghighirad, N. Sakai, L. Korte, B. Rech, M. B. Johnston, L. M. Herz, H. J. Snaith, *Science* **2016**, *351*, 151.

[148] N. H. Nickel, F. Lang, V. V. Brus, O. Shargaieva, J. Rappich, *Adv. Funct. Mater.* **2017**, *under revi*.

[149] T. Matsui, I. Petrikyte, T. Malinauskas, K. Domanski, M. Daskeviciene, M. Steponaitis, P. Gratia, W. Tress, J. P. Correa-Baena, A. Abate, A. Hagfeldt, M. Gr??tzel, M. K. Nazeeruddin, V. Getautis, M. Saliba, *ChemSusChem* **2016**, *9*, 2567.

[150] T. Dittrich, *Materials Concepts for Solar Cells*, Imperial College Press, London, **2014**.

[151] N. Onoda-Yamamuro, O. Yamamuro, T. Matsuo, H. Suga, *J. Phys. Chem. Solids* **1992**, *53*, 277.

[152] F. Brivio, J. M. Frost, J. M. Skelton, A. J. Jackson, O. J. Weber, M. T. Weller, A. R. Goñi, A. M. A. Leguy, P. R. F. Barnes, A. Walsh, *Phys. Rev. B* **2015**, *92*, 144308.

[153] H. Zhang, X. Qiao, Y. Shen, T. Moehl, S. M. Zakeeruddin, M. Grätzel, M. Wang, *J. Mater. Chem. A* **2015**, *3*, 11762.

[154] C. Quarti, E. Mosconi, J. M. Ball, V. D'Innocenzo, C. Tao, S. Pathak, H. J. Snaith, A. Petrozza, F. De Angelis, *Energy Environ. Sci.* **2016**, *9*, 155.

[155] T. J. Jacobsson, W. Tress, J.-P. Correa-Baena, T. Edvinsson, A. Hagfeldt, *J. Phys. Chem. C* **2016**, *120*, 11382.

[156] Y. Rong, L. Liu, A. Mei, X. Li, H. Han, *Adv. Energy Mater.* **2015**, *5*, 1.

[157] R. L. Milot, G. E. Eperon, H. J. Snaith, M. B. Johnston, L. M. Herz, *Adv. Funct. Mater.*

2015, *25*, 6218.

[158] Q. Ma, S. Huang, X. Wen, M. A. Green, A. W. Y. Ho-Baillie, *Adv. Energy Mater.* **2016**, *6*, 2.

[159] R. E. Beal, D. J. Slotcavage, T. Leijtens, A. R. Bowring, R. A. Belisle, W. H. Nguyen, G. F. Burkhard, E. T. Hoke, M. D. McGehee, *J. Phys. Chem. Lett.* **2016**, 746.

[160] A. Binek, F. C. Hanusch, P. Docampo, T. Bein, *J. Phys. Chem. Lett.* **2015**, *6*, 1249.

[161] N. J. Jeon, J. H. Noh, W. S. Yang, Y. C. Kim, S. Ryu, J. Seo, S. Il Seok, *Nature* **2015**, *517*, 476.

[162] K. Domanski, B. Roose, T. Matsui, M. Saliba, S.-H. Turren-Cruz, J.-P. Correa-Baena, C. R. Carmona, G. Richardson, J. M. Foster, F. De Angelis, J. M. Ball, A. Petrozza, N. Mine, M. K. Nazeeruddin, W. Tress, M. Grätzel, U. Steiner, A. Hagfeldt, A. Abate, *Energy Environ. Sci.* **2017**, *10*, 604.

[163] F. Huang, L. Jiang, A. R. Pascoe, Y. Yan, U. Bach, L. Spiccia, Y. B. Cheng, *Nano Energy* **2016**, *27*, 509.

[164] F. Zu, P. Amsalem, I. Salzmann, R. Wang, M. Ralaiarisoa, S. Kowarik, S. Duhm, N. Koch, *Adv. Opt. Mater.* **2017**, 1700139.

[165] V. Duzhko, V. Y. Timoshenko, F. Koch, T. Dittrich, *Phys. Rev. B* **2001**, *64*, 75204.

[166] K. Jemli, H. Diab, F. Lédée, G. Trippé-Allard, D. Garrot, B. Geffroy, J.-S. Lauret, P. Audebert, E. Deleporte, *Molecules* **2016**, *21*, 885.

[167] M. A. Pérez-Osorio, R. L. Milot, M. R. Filip, J. B. Patel, L. M. Herz, M. B. Johnston, F. Giustino, *J. Phys. Chem. C* **2015**, *119*, 25703.

[168] Y. Tian, M. Peter, E. L. Unger, M. Abdellah, K. Zheng, T. T. Pullerits, A. Yartsev, V. Sundstrom, I. G. Scheblykin, V. Sundström, I. G. Scheblykin, *Phys. Chem. Chem. Phys.* **2015**, *17*, 24978.

[169] A. J. Bard, R. Parsons, J. Jordan, *Standard Potentials in Aqueous Solution*, Taylor & Francis, **1985**.

[170] A. Miyata, A. Mitioglu, P. Plochocka, O. Portugall, J. T.-W. Wang, S. D. Stranks, H. J. Snaith, R. J. Nicholas, *Nat. Phys.* **2015**, *11*, 582.

[171] J. T. Jacobsson, J. P. Correa Baena, M. Pazoki, M. Saliba, K. Schenk, M. Grätzel, A. Hagfeldt, *Energy Environ. Sci.* **2016**, *41*, 1.

[172] S. T. Arroyo, A. H. Garcia, J. A. S. Martín, *Theor. Chem. Acc.* **2010**, *127*, 671.

[173] P. H. Joshi, L. Zhang, I. M. Hossain, H. A. Abbas, R. Kottokkaran, S. P. Nehra, M. Dhaka, M. Noack, V. L. Dalal, *AIP Adv.* **2016**, *6*, 115114.

[174] J. M. Azpiroz, E. Mosconi, J. Bisquert, F. De Angelis, *Energy Environ. Sci.* **2015**, *8*, 2118.

[175] F. Matsumoto, S. M. Vorpahl, J. Q. Banks, E. Sengupta, D. S. Ginger, *J. Phys. Chem. C* **2015**, *119*, 20810.

[176] R. Sheng, X. Wen, S. Huang, X. Hao, S. Chen, Y. Jiang, X. Deng, M. A. Green, A. W. Y. Ho-Baillie, *Nanoscale* **2016**, *8*, 1926.

[177] J. F. Galisteo-López, M. Anaya, M. E. Calvo, H. Míguez, *J. Phys. Chem. Lett.* **2015**, *6*, 2200.

[178] E. Mosconi, D. Meggiolaro, H. J. Snaith, S. D. Stranks, F. De Angelis, *Energy Environ. Sci.* **2016**, *9*, 3180.

[179] C. Zhao, B. Chen, X. Qiao, L. Luan, K. Lu, B. Hu, *Adv. Energy Mater.* **2015**, *5*, 1500279.

[180] E. Mosconi, F. De Angelis, *ACS Energy Lett.* **2016**, *1*, 182.

[181] R. Gottesman, L. Gouda, B. S. Kalanoor, E. Haltzi, S. Tirosh, E. Rosh-Hodesh, Y. Tischler, A. Zaban, C. Quarti, E. Mosconi, F. De Angelis, *J. Phys. Chem. Lett.* **2015**, *6*, 2332.

[182] Y. Yuan, J. Huang, *Acc. Chem. Res.* **2016**, *49*, 286.

[183] F. H. Taylor, J. Buckeridge, C. R. A. Catlow, *Chem. Mater.* **2016**, *28*, 8210.

[184] W. Tress, N. Marinova, T. Moehl, S. M. Zakeeruddin, N. Mohammad K., M. Grätzel,

M. K. Nazeeruddin, M. Grätzel, *Energy Environ. Sci.* **2015**, *8*, 995.

[185] T. Dittrich, J. Rappich, V. Y. Timoshenko, *Appl. Phys. Lett.* **1997**, *70*, 2705.

[186] V. Y. Timoshenko, a. B. Petrenko, M. N. Stolyarov, T. Dittrich, W. Fuessel, J. Rappich, *J. Appl. Phys.* **1999**, *85*, 4171.

[187] J. Wang, A. Zhang, J. Yan, D. Li, Y. Chen, *Appl. Phys. Lett.* **2017**, *110*, 123903.

[188] P. Delugas, A. Filippetti, A. Mattoni, *Phys. Rev. B* **2015**, *92*, 45301.

[189] V. M. Donnelly, A. P. Baronavski, J. R. McDonald, *Chem. Phys.* **1979**, *43*, 271.

[190] S. S. Prasad, L. A. Capone, *J. Geophys. Res.* **1976**, *81*, 5596.

[191] Y. H. Chang, C. H. Park, *J. Korean Phys. Soc.* **2004**, *44*, 889.

[192] Y. Wang, T. Gould, J. F. Dobson, H. Zhang, H. Yang, X. Yao, H. Zhao, *Phys. Chem. Chem. Phys.* **2014**, *16*, 1424.

[193] Z. Guo, Y. Wan, M. Yang, J. Snaider, K. Zhu, L. Huang, *Science* **2017**, *356*, 59.

[194] Y. Yang, D. P. Ostrowski, R. M. France, K. Zhu, J. van de Lagemaat, J. M. Luther, M. C. Beard, *Nat. Photonics* **2015**, *10*, 53.

[195] E. T. Hoke, D. J. Slotcavage, E. R. Dohner, A. R. Bowring, H. I. Karunadasa, M. D. McGehee, *Chem. Sci.* **2015**, *6*, 613.

[196] D. J. Slotcavage, H. I. Karunadasa, M. D. McGehee, *ACS Energy Lett.* **2016**, *1*, 1199.

[197] E. L. Unger, L. Kegelmann, K. Suchan, D. Sörell, L. Korte, S. Albrecht, *J. Mater. Chem. A* **2017**, DOI 10.1039/C7TA00404D.

[198] C. G. Bischak, C. L. Hetherington, H. Wu, S. Aloni, D. F. Ogletree, D. T. Limmer, N. S. Ginsberg, *Nano Lett.* **2017**, *17*, 1028.

[199] X. Yang, X. Yan, W. Wang, X. Zhu, H. Li, W. Ma, C. X. Sheng, *Org. Electron. physics, Mater. Appl.* **2016**, *34*, 79.

[200] F. Brivio, C. Caetano, A. Walsh, *J. Phys. Chem. Lett.* **2016**, *7*, 1083.

[201] P. Gratia, G. Grancini, J.-N. Audinot, X. Jeanbourquin, E. Mosconi, I. Zimmermann, D. Dowsett, Y. Lee, M. Grätzel, F. De Angelis, K. Sivula, T. Wirtz, M. K. Nazeeruddin, *J.*

Am. Chem. Soc. **2016**, *138*, 15821.

[202] J. Huang, P. Xu, J. Liu, X.-Z. You, *Small* **2017**, *13*, 1603225.

[203] D. Forgács, D. Pérez-del-Rey, J. Ávila, C. Momblona, L. Gil-Escrig, B. Dänekamp, M. Sessolo, H. J. Bolink, *J. Mater. Chem. A* **2017**, *5*, 3203.

[204] W. Liao, D. Zhao, Y. Yu, N. Shrestha, K. Ghimire, C. R. Grice, C. Wang, Y. Xiao, A. J. Cimaroli, R. J. Ellingson, N. J. Podraza, K. Zhu, R. G. Xiong, Y. Yan, *J. Am. Chem. Soc.* **2016**, *138*, 12360.

[205] W. Rehman, D. P. McMeekin, J. B. Patel, R. L. Milot, M. B. Johnston, H. J. Snaith, L. M. Herz, *Energy Environ. Sci.* **2017**, *10*, 361.

[206] G. E. Eperon, S. D. Stranks, C. Menelaou, M. B. Johnston, L. M. Herz, H. J. Snaith, *Energy Environ. Sci.* **2014**, *7*, 982.

[207] Z. Wu, B. Wang, J. He, T. Chen, *J. Colloid Interface Sci.* **2016**, *461*, 162.

[208] M. Kulbak, D. Cahen, G. Hodes, *J. Phys. Chem. Lett.* **2015**, *6*, 2452.

[209] T. J. Jacobsson, L. J. Schwan, M. Ottosson, A. Hagfeldt, T. Edvinsson, *Inorg. Chem.* **2015**, *54*, 10678.

[210] G. E. Eperon, C. E. Beck, H. J. Snaith, *Mater. Horiz.* **2016**, *3*, 63.

[211] R. J. Sutton, G. E. Eperon, L. Miranda, E. S. Parrott, B. A. Kamino, J. B. Patel, M. T. Hörantner, M. B. Johnston, A. A. Haghighirad, D. T. Moore, H. J. Snaith, *Adv. Energy Mater.* **2016**, *6*, 1502458.

[212] P. Fedeli, F. Gazza, D. Calestani, P. Ferro, T. Besagni, A. Zappettini, G. Calestani, E. Marchi, P. Ceroni, R. Mosca, *J. Phys. Chem. C* **2015**, *119*, 21304.

[213] J. H. Heo, D. H. Song, S. H. Im, *Adv. Mater.* **2014**, *26*, 8179.

[214] M. Hu, C. Bi, Y. Yuan, Y. Bai, J. Huang, *Adv. Sci.* **2016**, *3*, 1500301.

[215] J. R. Tesmer, M. A. Nastasi, M. Tesmer, J R;Nastasi, *Handbook of Modern Ion Beam Analysis*, Materials Research Society, Pittsburgh, Pennsilvania, **1995**.

[216] F. Lang, A. Juma, V. Somsongkul, T. Dittrich, M. Arunchaiya, *Hybrid Mater.* **2014**, *1*,

52.

[217] B. Li, Y. Chen, Z. Liang, D. Gao, W. Huang, *RSC Adv.* **2015**, *5*, 94290.

[218] D. Wei, T. Wang, J. Ji, M. Li, P. Cui, Y. Li, G. Li, J. M. Mbengue, D. Song, *J. Mater. Chem. A* **2016**, *4*, 1991.

[219] W. Qiu, U. W. Paetzold, R. Gehlhaar, V. Smirnov, H.-G. Boyen, J. G. Tait, B. Conings, W. Zhang, C. Nielsen, I. Mcculloch, L. Froyen, P. Heremans, D. Cheyns, *J. Mater. Chem. A* **2015**, 22824.

[220] H. Xie, X. Liu, L. Lyu, D. Niu, Q. Wang, J. Huang, Y. Gao, *J. Phys. Chem. C* **2016**, *120*, 215.

[221] F. Matteocci, Y. Busby, J.-J. Pireaux, G. Divitini, S. Cacovich, C. Ducati, A. Di Carlo, *ACS Appl. Mater. Interfaces* **2015**, *7*, 26176.

[222] A. Calloni, A. Abate, G. Bussetti, G. Berti, R. Yivlialin, F. Ciccacci, L. Duò, *J. Phys. Chem. C* **2015**, *119*, 21329.

[223] H. Xu, Y. Wu, J. Cui, C. Ni, F. Xu, J. Cai, F. Hong, Z. Fang, W. Wang, J. Zhu, L. Wang, R. Xu, F. Xu, *Phys. Chem. Chem. Phys.* **2016**, *18*, 18607.

[224] W. A. Dunlap-Shohl, R. Younts, B. Gautam, K. Gundogdu, D. B. Mitzi, *J. Phys. Chem. C* **2016**, *120*, 16437.

[225] Y. Liu, L. A. Renna, M. Bag, Z. A. Page, P. Kim, J. Choi, T. Emrick, D. Venkataraman, T. P. Russell, *ACS Appl. Mater. Interfaces* **2016**, *8*, 7070.

[226] U. Bansode, R. Naphade, O. Game, S. Agarkar, S. Ogale, *J. Phys. Chem. C* **2015**, *119*, 9177.

[227] P. Luo, Z. Liu, W. Xia, C. Yuan, J. Cheng, Y. Lu, *J. Mater. Chem. A* **2015**, *3*, 12443.

[228] J. A. McLeod, Z. Wu, P. Shen, B. Sun, L. Liu, *J. Phys. Chem. Lett.* **2014**, *5*, 2863.

[229] J. Emara, T. Schnier, N. Pourdavoud, T. Riedl, K. Meerholz, S. Olthof, *Adv. Mater.* **2016**, *28*, 553.

[230] B. Philippe, B.-W. Park, R. Lindblad, J. Oscarsson, S. Ahmadi, E. M. J. Johansson, H.

Rensmo, *Chem. Mater.* **2015**, *27*, 1720.

[231] R. Lindblad, D. Bi, B. Park, J. Oscarsson, M. Gorgoi, H. Siegbahn, M. Odelius, E. M. J. Johansson, H. Rensmo, *J. Phys. Chem. Lett.* **2014**, *5*, 648.

[232] B. Conings, L. Baeten, C. De Dobbelaere, J. D'Haen, J. Manca, H.-G. Boyen, *Adv. Mater.* **2014**, *26*, 2041.

[233] G. Sadoughi, D. E. Starr, E. Handick, S. D. Stranks, M. Gorgoi, R. G. Wilks, M. Bär, H. J. Snaith, *ACS Appl. Mater. Interfaces* **2015**, *7*, 13440.

[234] Y. Zhou, A. L. Vasiliev, W. Wu, M. Yang, S. Pang, K. Zhu, N. P. Padture, *J. Phys. Chem. Lett.* **2015**, *6*, 2292.

[235] E. Edri, S. Kirmayer, S. Mukhopadhyay, K. Gartsman, G. Hodes, D. Cahen, *Nat. Commun.* **2014**, *5*, 3461.

[236] H. Yuan, E. Debroye, K. Janssen, H. Naiki, C. Steuwe, G. Lu, M. Moris, E. Orgiu, H. Uji-i, F. De Schryver, P. Samorì, J. Hofkens, M. Roeffaers, *J. Phys. Chem. Lett.* **2016**, *7*, 561.

[237] N. Kedem, T. M. Brenner, M. Kulbak, N. Schaefer, S. Levcenko, I. Levine, D. Abou-Ras, G. Hodes, D. Cahen, *J. Phys. Chem. Lett.* **2015**, 150610174034007.

[238] B. Todd, S. Uznanski, *CAS - Cern Accel. Sch. Power Convert.* **2015**, *3*, 1.

[239] J. J. Loferski, P. Rappaport, *Phys. Rev.* **1958**, *111*, 432.

[240] J. R. Srour, C. J. Marshall, P. W. Marshall, *IEEE Trans. Nucl. Sci.* **2003**, *50*, 653.

[241] T. Markvart, *J. Mater. Sci. Mater. Electron.* **1990**, *1*, 1.

[242] E. J. Daly, G. Drolshagen, A. Hilgers, H. D. R. Evans, *Environ. Model. Space-based Appl. Symp. Proc.* **1996**, 15.

[243] H. C. Neitzert, P. Spinillo, S. Bellone, G. D. Licciardi, M. Tucci, F. Roca, L. Gialanella, M. Romano, *Sol. Energy Mater. Sol. Cells* **2004**, *83*, 435.

[244] S. R. Messenger, G. P. Summers, E. A. Burke, R. J. Walters, M. A. Xapsos, *Prog. Photovoltaics Res. Appl.* **2001**, *9*, 103.

[245] M. Alurralde, M. J. L. Tamasi, C. J. Bruno, M. G. Marťnez Bogado, J. Plá, J. Fernández Vázquez, J. Durán, J. Schuff, A. A. Burlon, P. Stoliar, A. J. Kreiner, *Sol. Energy Mater. Sol. Cells* **2004**, *82*, 531.

[246] A. D. Verkerk, J. K. Rath, R. E. I. Schropp, *Proc. Inorg. Nanostructured Photovoltaics* **2010**, *2*, 221.

[247] R. A. Street, J. E. Northrup, B. S. Krusor, *Phys. Rev. B - Condens. Matter Mater. Phys.* **2012**, *85*, 1.

[248] F. Bebensee, J. Zhu, J. H. Baricuatro, J. A. Farmer, Y. Bai, H. P. Steinrück, C. T. Campbell, J. M. Gottfried, *Langmuir* **2010**, *26*, 9632.

[249] D. A. Egger, L. Kronik, A. M. Rappe, *Angew. Chemie Int. Ed.* **2015**, *54*, 12437.

[250] H. L. Wells, *Zeitschrift für Anorg. Chemie* **1893**, *3*, 195.

[251] H. Haupt, F. Huber, H. Preut, *Zeitschrift für Anorg. und Allg. Chemie* **1974**, *408*, 209.

[252] I. Chung, J.-H. Song, J. Im, J. Androulakis, C. D. Malliakas, H. Li, A. J. Freeman, J. T. Kenney, M. G. Kanatzidis, *J. Am. Chem. Soc.* **2012**, *134*, 8579.

[253] S. Bai, Z. Yuan, F. Gao, *J. Mater. Chem. C* **2016**, *4*, 3898.

[254] L. Protesescu, S. Yakunin, M. I. Bodnarchuk, F. Krieg, R. Caputo, C. H. Hendon, R. X. Yang, A. Walsh, M. V. Kovalenko, *Nano Lett.* **2015**, *15*, 3692.

[255] M. C. Tathavadekar, S. A. Agarkar, O. S. Game, U. P. Bansode, S. A. Kulkarni, S. G. Mhaisalkar, S. B. Ogale, *Sol. Energy* **2015**, *112*, 12.

[256] J. Liang, C. Wang, Y. Wang, Z. Xu, Z. Lu, Y. Ma, H. Zhu, Y. Hu, C. Xiao, X. Yi, G. Zhu, H. Lv, L. Ma, T. Chen, Z. Tie, Z. Jin, J. Liu, *J. Am. Chem. Soc.* **2016**, *138*, 15829.

[257] L. A. Frolova, D. V. Anokhin, A. A. Piryazev, S. Y. Luchkin, N. N. Dremova, K. J. Stevenson, P. A. Troshin, *J. Phys. Chem. Lett.* **2017**, *8*, 67.

[258] R. E. Brandt, V. Stevanović, D. S. Ginley, T. Buonassisi, *MRS Commun.* **2015**, *5*, 1.

[259] S. Chakraborty, W. Xie, N. Mathews, M. Sherburne, R. Ahuja, M. Asta, S. G. Mhaisalkar, *ACS Energy Lett.* **2017**, *2*, 837.

[260] L. A. Frolova, D. V. Anokhin, A. A. Piryazev, S. Y. Luchkin, N. N. Dremova, P. A. Troshin, *J. Phys. Chem. Lett.* **2017**, *8*, 1651.

[261] Y. Kim, Z. Yang, A. Jain, O. Voznyy, G.-H. Kim, M. Liu, L. N. Quan, F. P. García de Arquer, R. Comin, J. Z. Fan, E. H. Sargent, *Angew. Chemie Int. Ed.* **2016**, *55*, 9586.

[262] G. Volonakis, M. R. Filip, A. A. Haghighirad, N. Sakai, B. Wenger, H. J. Snaith, F. Giustino, *J. Phys. Chem. Lett.* **2016**, *7*, 1254.

[263] G. Volonakis, A. A. Haghighirad, R. L. Milot, W. H. Sio, M. R. Filip, B. Wenger, M. B. Johnston, L. M. Herz, H. J. Snaith, F. Giustino, *J. Phys. Chem. Lett.* **2017**, *8*, 772.

[264] F. Giustino, H. J. Snaith, *ACS Energy Lett.* **2016**, *1*, 1233.

[265] A. H. Slavney, T. Hu, A. M. Lindenberg, H. I. Karunadasa, *J. Am. Chem. Soc.* **2016**, *138*, 2138.

[266] E. T. Mcclure, M. R. Ball, W. Windl, P. M. Woodward, *Chem. Mater.* **2016**, *28*, 1348.

[267] W. Li, Z. Wang, F. Deschler, S. Gao, R. H. Friend, A. K. Cheetham, *Nat. Rev. Mater.* **2017**, *2*, 16099.

[268] G. Kieslich, S. Sun, A. K. Cheetham, *Chem. Sci.* **2015**, *6*, 3430.

((**For Essays, Feature Articles, Progress Reports, and Reviews,** please insert up to three author biographies and photographs here, max. 100 words each))

Author Photograph(s) ((40 mm broad, 50 mm high, gray scale))

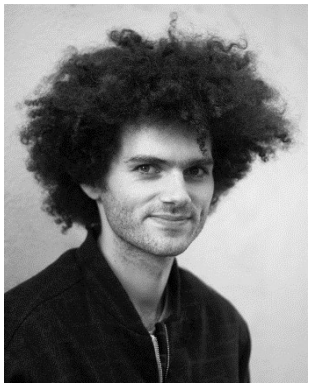

Felix Lang received his Bachelor degree in Applied and Engineering Physics in 2012 from the Technische Universität München, while working on organic bulk heterojunction solar cells. He received his Master degree in Physics in 2014 from the Freie Universität Berlin, working with Dr. T. Dittrich on perovskite solar cells. Currently he is a doctoral candidate under supervision of Prof. Dr. N. H Nickel at the Helmholtz-Zentrum Berlin für Materialien und Energie GmbH. His research interests range from functional materials, their physical properties to novel device concepts.

Oleksandra Shargaieva studied organic chemistry at Taras Shevchenko National University of Kyiv. She received her Master degree in Chemistry in 2014, working on supramolecular interactions of polymethine dyes. Currently she is a member of the graduate school Hybrid 4 Energy, working under supervision of Prof. Dr. N. H Nickel at the Helmholtz-Zentrum Berlin für Materialien und Energie GmbH. Her main scientific interests are synthesis, spectroscopy, and application of hybrid perovskites.

T_{80} lifetimes of organic-inorganic perovskite solar cells are strongly reduced under illumination. Various degradation mechanisms are therefore discussed throughout literature. Degradation by moisture or heat is well understood and mitigation possible. Photo-induced phase segregation and photo-induced dissociation of the organic cation however remain unsolved. Recent observations enlighten the underlying microscopic mechanisms and may pave the way for stable perovskites.

Keyword

Felix Lang*, Oleksandra Shargaieva, Viktor V. Brus, Jörg Rappich, Norbert H. Nickel

Title ((no stars))

ToC figure